AFATL-TR-84-89

Friction of Plastic Rotating Bands

A K Stiffler

MISSISSIPPI STATE UNIVERSITY
DEPT OF MECHANICAL & NUCLEAR ENGINEERING
P O DRAWER ME
MISSISSIPPI STATE, MS 39762

NOVEMBER 1984

FINAL REPORT FOR PERIOD AUGUST 1982–SEPTEMBER 1984

Approved for public release; distribution is unlimited

20000807021

Air Force Armament Laboratory
AIR FORCE SYSTEMS COMMAND • UNITED STATES AIR FORCE • EGLIN AIR FORCE BASE, FLORIDA

NOTICE

Please do not request copies of this report from the Air Force Armament Laboratory. Additional copies may be purchased from:

National Technical Information Service
5285 Port Royal Road
Springfield, Virginia 22161

Federal Government agencies and their contractors registered with Defense Technical Information Center should direct requests for copies of this report to:

Defense Technical Information Center
Cameron Station
Alexandria, Virginia 22314

UNCLASSIFIED

SECURITY CLASSIFICATION OF THIS PAGE (When Data Entered)

REPORT DOCUMENTATION PAGE AD-A150666	READ INSTRUCTIONS BEFORE COMPLETING FORM
1. REPORT NUMBER AFATL-TR-84-89	2. GOVT ACCESSION NO. [redacted] 3. RECIPIENT'S CATALOG NUMBER
4. TITLE (and Subtitle) FRICTION OF PLASTIC ROTATING BANDS	5. TYPE OF REPORT & PERIOD COVERED Final Report: August 1982-September 1984 6. PERFORMING ORG. REPORT NUMBER AKS-84-1
7. AUTHOR(s) A. Kent Stiffler	8. CONTRACT OR GRANT NUMBER(s) F08635-82-K-0261
9. PERFORMING ORGANIZATION NAME AND ADDRESS Mississippi State University, Engineering and Industrial Research Station, Drawer DE, Mississippi State, Mississippi 39762	10. PROGRAM ELEMENT, PROJECT, TASK AREA & WORK UNIT NUMBERS PE: 62602F JON: 2308-E1-11
11. CONTROLLING OFFICE NAME AND ADDRESS Air Force Armament Laboratory (DLJG) Armament Division Eglin Air Force Base, Florida 32542	12. REPORT DATE November 1984 13. NUMBER OF PAGES 110
14. MONITORING AGENCY NAME & ADDRESS(if different from Controlling Office)	15. SECURITY CLASS. (of this report) Unclassified 15a. DECLASSIFICATION/DOWNGRADING SCHEDULE

16. DISTRIBUTION STATEMENT (of this Report)

APPROVED FOR PUBLIC RELEASE; DISTRIBUTION UNLIMITED.

17. DISTRIBUTION STATEMENT (of the abstract entered in Block 20, if different from Report)

18. SUPPLEMENTARY NOTES

Availability of this report is specified on verso of front cover.

19. KEY WORDS (Continue on reverse side if necessary and identify by block number)

Rotating Bands
Friction
Interior Ballistics

20. ABSTRACT (Continue on reverse side if necessary and identify by block number)

A melt concept is proposed to explain the friction and wear of unlubricated contacts subjected to high loads and sliding speeds. A theory is derived to calculate the sliding force between metal rotating bands and rifling in interior ballistics. Expressions are given for

DD FORM 1 JAN 73 1473 EDITION OF 1 NOV 65 IS OBSOLETE

UNCLASSIFIED

SECURITY CLASSIFICATION OF THIS PAGE (When Data Entered)

film thickness, temperature, coefficient of friction, and band wear. An example is presented for copper rotating bands.

The above theory is extended to pin-on-disk devices which are the primary source of friction data. Good agreement with early Franklin Institute data at high sliding speeds validated the theoretical approach.

A complete review of polymer friction and the rheology of non-Newtonian polymer melt behavior is given. A limiting shear stress concept is justified for polymers and forms the basis of a non-Newtonian melt rheology model. A melt friction theory is derived for plastic rotating bands.

PREFACE

This program was conducted by the Mississippi State University, Engineering and Industrial Research Station, P. O. Drawer DE, Mississippi State, Mississippi 39762, under Contract FO8635-82-K-0261 with the Air Force Armament Laboratory, Armament Division, Eglin Air Force Base, Florida 32542. Lieutenant James Schoeneman (DLJG) was the program officer for the Armament Laboratory. The program was conducted during the period from August 1982 to September 1984.

The author wishes to thank O.K. Heiney, Chief of the Propellants and Interior Ballistics Group, Air Force Armament Laboratory, for his continual interest, encouragement, and instruction in experimental interior ballistics.

The Public Affairs Office has reviewed this report, and it is releasable to the National Technical Information Service (NTIS), where it will be available to the general public, including foreign nationals.

This technical report has been reviewed and is approved for publication.

FOR THE COMMANDER

Milton D. Kingcaid

MILTON D. KINGCAID, Colonel, USAF
Chief, Munitions Division

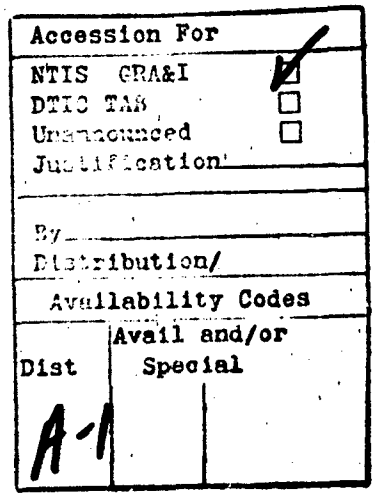

(The reverse of this page is blank.)

TABLE OF CONTENTS

TABLE OF CONTENTS (CONCLUDED)

LIST OF FIGURES

LIST OF FIGURES (CONCLUDED)

LIST OF TABLES

NOMENCLATURE

a	asperity contact radius
A	slider area
A_r	real area of microcontacts
B	slider length in z direction
c	specific heat
E	Youngs modulus
f	coefficient of friction
$\bar{f}$	ratio of experimental to theoretical f
G	elastic shear modulus
h	melt thickness
H	heat of fusion
H_r	disk hardness
k	thermal conductivity of melt
k'	thermal conductivity of solid
ℓ	short side length of slider
ℓ_c	characteristic length of contact
L	slider length in x direction
$\dot{m}$	mass melt rate per unit area of slider or fixed surface
p	pressure
q	heat flux per unit area
r	radial coordinate of pin
R	pin radius
R	Reynolds' number
s	solid shear stress
t	time
T	temperature
T_o	initial temperature
u	velocity in the x direction
U	slider velocity
v	velocity in the y direction
v_r	pin melt velocity in x direction
v_x	pin melt velocity in r direction
V	volume of melt per unit sliding distance
w	velocity in the z direction

W	load on slider
x	direction of slider motion
x_o	slider displacement
y	direction $\perp$ to melt plane
z	direction in melt plane $\perp$ to x
α	diffusivity or viscosity pressure coefficient or viscosity temperature coefficient
β	ratio of width to short side length or viscosity temperature coefficient
δ	equation (64)
γ	shear stress pressure coefficient
κ	shear modulus pressure coefficient
μ	absolute viscosity of melt or friction coefficient in literature review
ρ	mass density
σ	load per unit area
σ_f	flow pressure (also p_m)
τ	fluid shear stress
τ_L	limiting shear stress

Superscript

'	properties of non-melting solid

Subscript

s	slider surface
f	fixed surface
m	melt surface
nm	non-melt surface

(The reverse of this page is blank.)

SECTION I

INTRODUCTION

The basic interior ballistic problem is to determine the energy release and corresponding pressure generated by the burning propellant in a variable volume, ultimately to establish the muzzle velocity of the projectile. The dynamics must account for certain losses which include rotating band frictional effects and heat transfer from the hot gases to the gun. Krier and Adams [1] report that frictional losses account for approximately two percent of the energy released by the propellants in medium caliber guns. Although direct friction losses appear small, they are important where an accurate prediction of projectile velocity is desired. Friction can indirectly influence the thermodynamics and heat transfer processes which play a much larger role in the projectile velocity. Small changes in the initial engraving forces can increase the peak gas pressures and temperatures by twenty percent [2].

Another problem in internal ballistics is gun life. Both erosion and wear can lead to barrel replacement after a few thousand rounds [3]. In the past rotating bands have been made from bronze (90 CU, 10 ZN), called gilding metal; however, recent success [4] with nylon bands suggest that they will be used extensively in the future. Plastic bands not only reduce sliding forces but improve gun life. The need for better velocity predictive codes and for an understanding of barrel wear has intensified interest in rotating band contact loads and sliding forces.

Frictional behavior in internal ballistics is exceedingly complex due to the large loading forces, high sliding velocities, and the nature of the dynamically changing interface between the projectile and barrel. Engraving and bore sliding force equations take essentially two forms. In the closed form models [5] the friction is assumed to be proportional to the kinetic velocity of the projectile. In open form models a table of resistance force as a function of projectile position is used or, more simply, a constant engraving force followed by a smaller constant bore force [6]. Estimates of these two forces are

given as 10% and 1% of the maximum gas pressure. Recently, Fisher and Trippe [7] have divided the friction force into a linearly increasing force during the engraving process followed by a linearly decreasing force during the bore sliding process. This model is based upon data obtained from extruding brass and aluminum stock. In all cases empirical sliding forces are based on ad hoc conditions.

1. THE PROBLEM

Recently [8], the writer has developed a theory for the normal loads and sliding forces encountered by projectiles when their rotating bands (plastic) are engraved. The theory illustrated the need to consider geometrical details and served to isolate the dynamic flow pressure and the coefficient of friction as the main parameters. The theory also accounted for band radial displacements. These displacements are caused by normal loads on flexible walled projectiles and by propellant gas pressures which produce radial strain in the projectile and barrel. Finally, the theory was extended to determine the normal loads between the projectile and barrel for the post-engraving region of contact.

An application of the theory requires a knowledge of sliding friction as a function of load and velocity. Generally, this information is available only for selected materials and loads. The effect of velocity on the coefficient of friction has been one of the more neglected areas of research in tribology. In most cases the coefficient of friction decreases with velocity. Above a certain PV (pressure x velocity) the coefficient of friction drops to a value substantially less than 0.1 and remains constant. The critical PV value for bronze rotating bands is approximately 4×10^6 (psi)(fps), and Montgomery [9][10][11] identifies this equilibrium region with material melting. Since polymers melt at much lower temperatures than bronze, it is probable that most of the band engraving takes place in this equilibrium region. When Stiffler's engraving theory [8] was applied to the experimental work of Cross, it was found that the coefficient of friction for plastic bands was on the order of 0.02.

It is proposed to develop a theory of friction for plastic rotating bands in interior ballistics. Section II reviews the present understanding of friction in the scientific community. Section III

reviews the rheology of both Newtonian and non-Newtonian fluid mechanics since the underlying phenomenon centers about a melt layer between surfaces. Section IV develops a new melt friction theory which is applied to metal rotating bands (Newtonian melt). The theory is used to explain the rotating band data of Montgomery [9-10]. This section is a self-contained paper [12] accepted for publication in the ASME Journal of Tribology. Section V extends the theory to the circular contact of pin-on-disk devices which are the main source of friction data. A comparison with the high speed Franklin Institute data [11] further validates the theoretical approach to plastic rotating bands. This chapter has been submitted for review to the Journal of Tribology [13]. Section VI develops the theory for plastic rotating bands which requires a major adaption for non-Newtonian polymer melts.

(The reverse of this page is blank.)

SECTION II

LITERATURE REVIEW OF FRICTION

1. FRICTION (GENERAL)

The basic mechanism of friction is now well established [14], particularly for metals. It is known that, when two surfaces are placed together, intimate contact occurs only at the tips of the asperities in the surface. These asperities are then deformed plastically until the real area of contact A_r is sufficient to support the load W. Over this contact area there is marked molecular interaction so that a cold weld or junction is formed which is comparable in strength to the bulk material forming the junctions. In sliding, a certain force F is required to shear these minute junctions. Thus,

$$F = A_r s \tag{1}$$

where s is the shear strength of the junction. Since

$$A_r = \frac{W}{p_m} \tag{2}$$

where p_m is the material flow pressure, the coefficient of friction

$$\mu = \frac{s}{p_m} \tag{3}$$

Although this model explains the main characteristics of metallic friction, the value of the friction coefficient calculated from material strength properties are somewhat lower ($\mu = 0.2$) than the value found in practice ($\mu = 1.0$). The reason for the discrepancy was first explained by McFarlane and Tabor [15]. As sliding commences at an asperity junction, the real area of contact can increase several fold. This is because the condition for plastic yielding of a junction is determined by the combined effect of the normal stress p and the tangential stress s, the yield criterion being

$$p^2 + \gamma s^2 = p_o^2 \tag{4}$$

where p_o is the initial static contact pressure, and Y is a constant with a value of about ten. As soon as a tangential force is applied, p diminishes with a corresponding increase in the contact area.

2. POLYMER FRICTION (LOAD)

One of the first studies of polymer friction, Shooter and Tabor [16], showed that strong adhesion occurs at the sliding surface and that over a restricted range of loads frictional behavior is approximately expressed in terms of equation (3). Howell and Mazur [17] pressed polymer fibers against a flat plate and reported that friction does not increase linearly with load:

$$F \sim W^n \qquad (5)$$

where $n < 1$. Thus, the coefficient of friction decreased as the load increased. They interpreted this result as meaning that the real area of contact followed a law of the type: $A \sim W^n$. Pascoe and Tabor [18] investigated the friction of crossed polymer fibers (diameter D mm) at very light loads and confirmed that

$$\mu \sim W^{-m} \qquad (6)$$

(Figure 1). In contrast to metals there appeared to be little or no junction growth during sliding. No distinction was made between the real contact area and the apparent contact area. A very thorough study of nylon friction was carried out by Adams [19][20]. He slid nylon 6-10 hemispheres (diameters: 0.24 - 1.16 cm) on a smooth glass surface, using speeds from 10^{-7} to 3×10^{-2} cm/sec and loads from 0.7 to 200 g. His measurements showed that the load dependence of both the apparent contact area and the friction force could be represented by the expressions:

$$A = \beta W^m \qquad (7)$$

and

$$F = \alpha W^n \qquad (8)$$

where β and α are constants. The values of m and n were independent of specimen radius and were given by 0.708 and 0.781, respectively. Adams proposed that the increase of F/A with load could be explained either by an increase in the ratio of true to apparent contact area with load

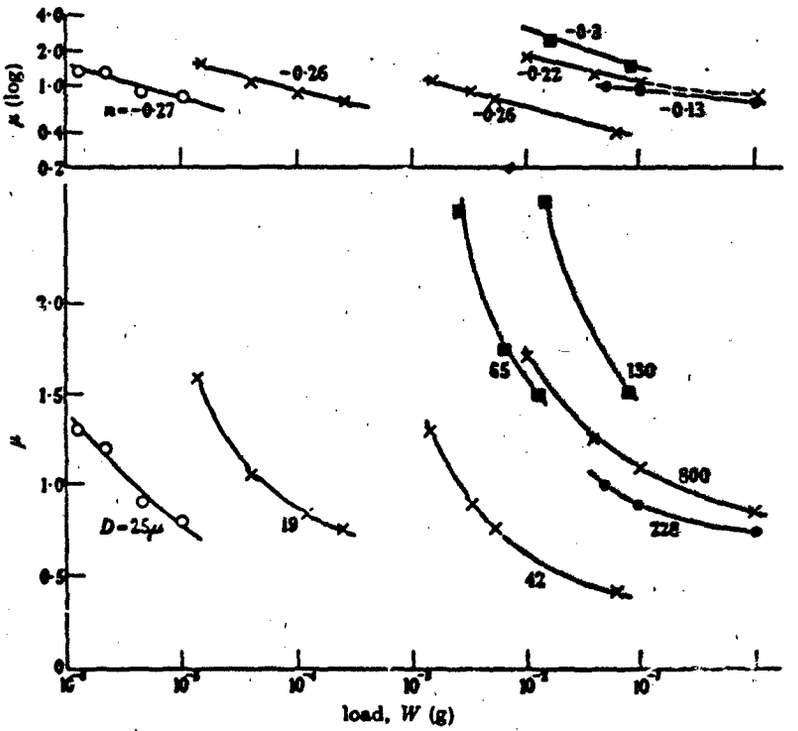

Figure 1. Friction of Fibers as a Function of Load

while the shear strength of the true contact area remained constant, or by an increase of this shear strength with pressure. After detailed considerations, he concluded the latter was more likely.

3. AREA OF CONTACT

It was initially accepted that all contacting asperities deform plastically since Amontons' laws of friction would be violated if the contacts were elastic, i.e., $A_r \sim W^{2/3}$ from Hertzian contact of a single asperity. However, Lodge and Howell [21] and Archard [22] proved that multiple contacts with elastic asperities will produce a real contact area which is nearly proportional to the load. Lodge and Howell assumed a spherical surface of very small hemispheres of constant height (Figure 2). For elastic deformation the real area of contact turned out to be $A_r \sim W^{8/9}$. Archard allowed for asperities of variable heights and found that $A \sim W^{.86}$. Furthermore, Archard showed that, if the asperities are covered by smaller asperities, $A \sim W^{26/27}$. In general, both elastic and plastic deformations probably occur. Plastic deformations predominate with rough surfaces and large loads.

For polymers subjected to small loads the apparent contact area between a hard surface and polymer sphere is given by $A \sim W^{(2m-m)}$. Thus, real areas of contact for polymers are essentially proportional to the load even when viscoelastic deformation of asperities occur.

4. POLYMER FRICTION (LOW SPEED)

In the conventional presentation of the adhesion theory of friction, it is assumed that the small contact area increases with the load in a way that the average contact stress remains constant and equal to the flow strength of the softer material. Then the shear strength of the junctions can be treated as invariant. Thus, the friction coefficient is constant and independent of load as required by Amontons' law. However, polymers do not obey Amontons' law. A number of different workers [24][25][26][27][28], taking the lead of Adams, verified that the strength properties of polymers, unlike metals, increased with the hydrostatic pressure. Towle [29][30] proposed a simple extension of adhesion theory. If the shear stress

$$s = s_o + \alpha p \quad , \tag{9}$$

it follows that

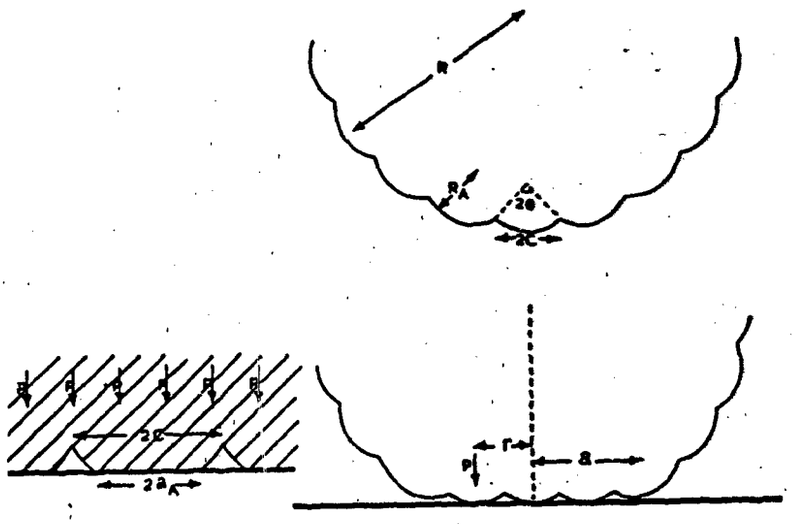

Figure 2. Model of Surface Roughness

$$s = s_o + \alpha p \quad .$$

it follows that

$$\mu = \frac{s}{p} + \alpha \qquad (10)$$

The equation predicts that the friction coefficient decreases with increasing load (pressure), approaching an asymptotic value at high loads. Towle [30] states: "for many metals the parameter α is very small, typically ~0.01, while for polymers it is sometimes an order of magnitude larger." He found that $\alpha = 0.07$ for the phosphinate (Figure 3). The agreement between experimental values of friction coefficient and the above model is excellent. At low loads the area contacts are partial, but at high loads the real area of contact approaches the apparent area of contact. The contact stress p_c at which the transition from low load to high load occurs can be shown to be [30]

$$p_c = \left[\frac{1}{p_m} - \frac{\alpha}{s_o} \right]^{-1} \qquad (11)$$

According to plasticity theory the bulk flow pressure p_m should be about five times the bulk shear strength of the material. Then the transition stress is

$$p_c = \frac{s_o}{(0.2 - \alpha)} \qquad (12)$$

Peterson and Ling [31] suggested a relationship similar to equation (10) for metals. Generally, the coefficient of friction was independent of load, obeying Amontons' law, until loads were sufficiently high to produce gross deformations as with metalworking processes. Their values of $\alpha = 0.11$ for aluminum contradicts the statement of Towle that α is small for metals. Undoubtedly, the transition stress for metals occurs at levels outside of typical engineering applications and experimental friction studies.

Briscoe and Tabor [27] studied the effect of pressure on the shear properties of very thin films. They found that the shear strength of thin films is much less than the shear strength of the bulk polymer. However, the asymptotic friction coefficient α showed little difference. It is apparent that the constants s_o and α can vary with

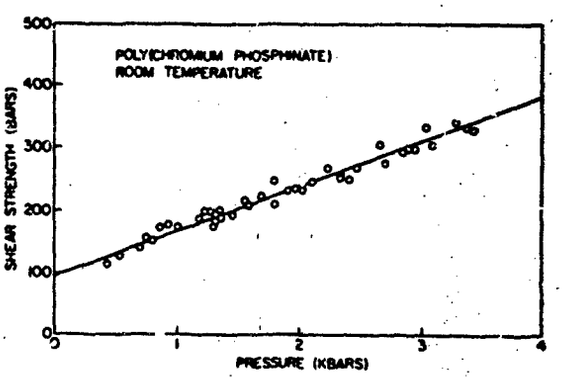

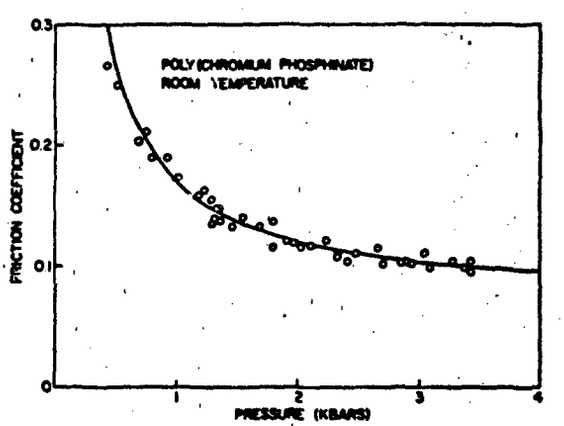

Figure 3. Shear Strength and Friction Coefficient of Poly (Chromium Phosphinate)

sliding velocity since contact temperatures increase with frictional energy dissipation. Briscoe and Tabor [27] reported that the shear strength of polymethylmethacrylate (PMMA) abruptly dropped when test temperatures reached the glass transition temperature (Figure 4).

Ludema and Tabor [32] found a pronounced variation in the sliding friction of polymers with temperature and speed (less than 1 cm/sec). There is a dramatic decrease in junction shear strength s and increase in contact area A for temperatures up to 150°C (Figure 5). The product sA, which is the friction force, leads to unpredictable behavior in the coefficient of friction. The effect of speed (10^{-4} to 1 cm/sec) on the coefficient of friction is minimal for nylon 6-6 but is substantial for polythene (Figure 6). The reader may contrast the above speed effect on nylon 6-6 with the results of Adams for nylon 6-10 (Figure 7).

5. POLYMER FRICTION (MEDIUM SPEED)

When two surfaces are in relative motion, the frictional work will be liberated as heat at the surface asperities. Thus, temperature effects should be more pronounced at higher sliding speeds. Bowden and Tabor [14] obtained experimental evidence for surface contact temperatures as high as 1000°C with constantan sliding on steel. With other metals the peak temperatures recorded corresponded to their melting points. It was noted that lubricants, although reducing the peak temperatures, did not prevent hot spots from occurring. Also, the sliding of poor conductors resulted in correspondingly higher surface temperatures.

From elementary considerations the rate of friction work must be equal to the rate of heat transfer to the material bulk:

$$WU\mu = cA(\Delta T) \tag{13}$$

where c is a constant which is a function of the thermal conductivity k. If the temperature change is limited to the material melting point, the above equation can be rearranged to the form: pressure x velocity = constant, the limit equation for bearing failure.

Jaeger [33] has given an equation for calculating the surface temperature of a single asperity contact of radius R_o:

$$\Delta T = \frac{\mu W U g}{4.24\ R_o(k_1 + k_2)} \tag{14}$$

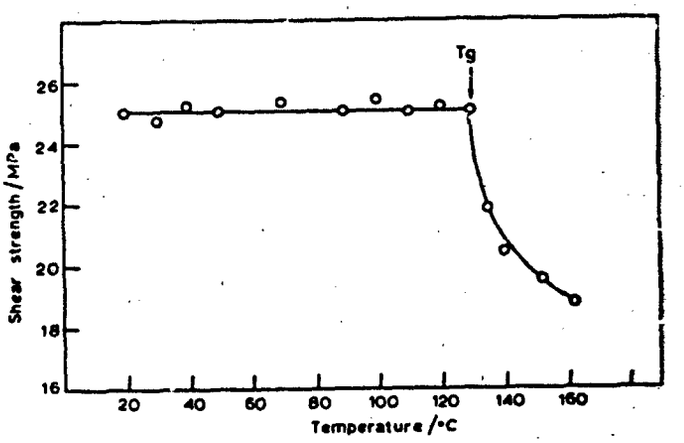

Figure 4. Shear Strength as a Function of Temperature for PMMA Films at a Contact Pressure of 2×10^8 Pa and a Sliding Velocity of 0.03 mms^{-1}

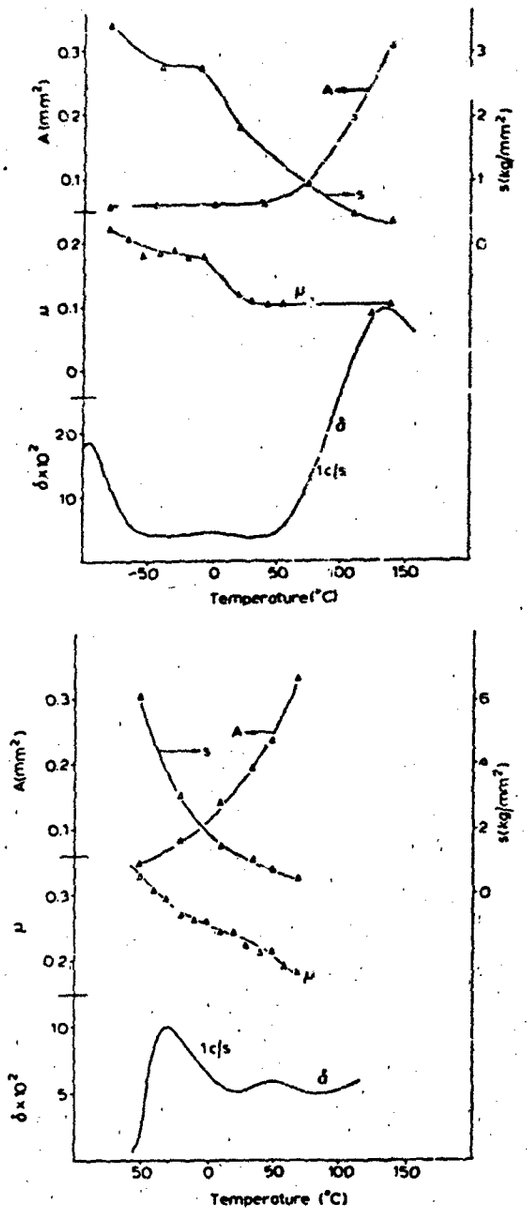

Figure 5. Coefficient of Friction, Area of Contact and Shear Strength for a Hard Steel Slider on (POM) and (PP) as a Function of a Temperature. Sliding Speed 0.035 cm/sec

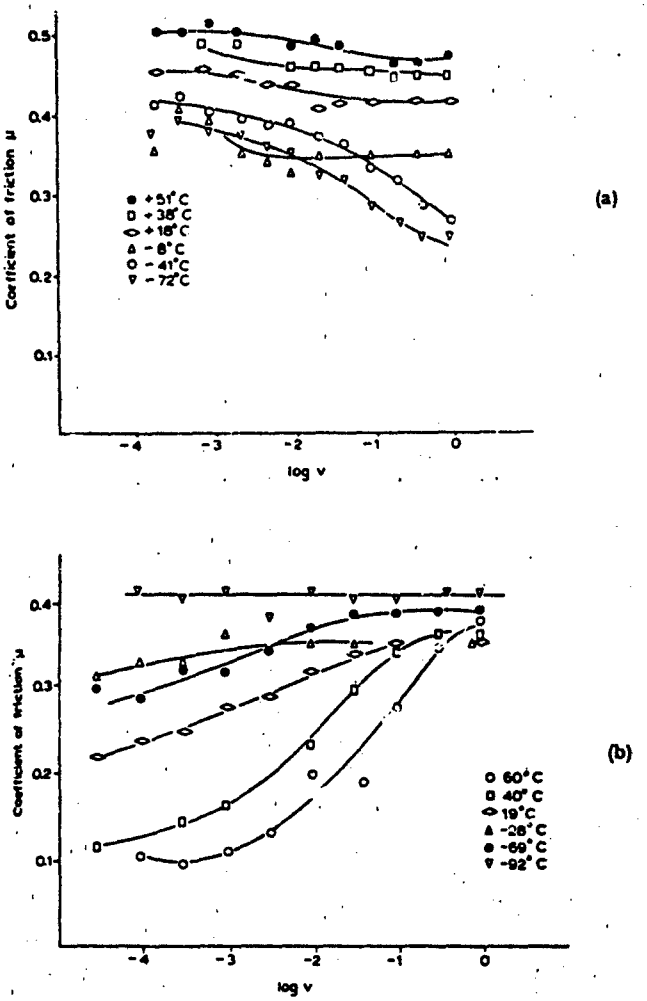

Figure 6. Sliding Friction of a Hard Steel Slider Over (a) Nylon and (b) Polythrene as a function of Speed and Temperature

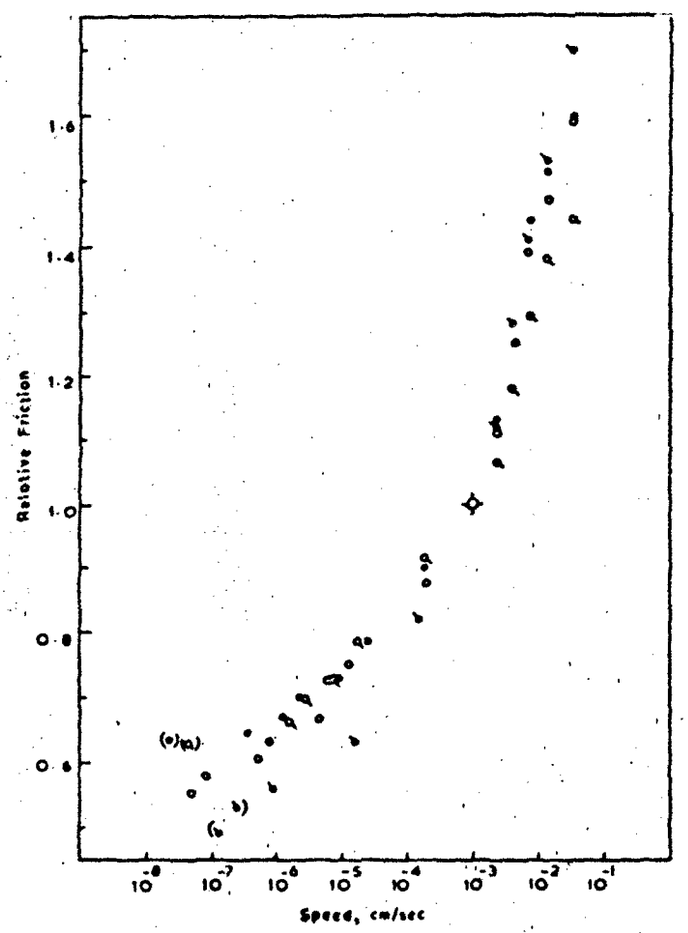

Figure 7. Speed Variation of Friction

Following Jaeger, Archard [34] found that, for plastic deformation and low speeds ($L < .1$),

$$\Delta T = \frac{\mu(\pi p_m)^{1/2} W^{1/2} U}{8k} \tag{15}$$

and that, for plastic deformation and high speeds ($L > 100$),

$$\Delta T = \frac{\mu(\pi p_m)^{3/4} W^{1/4} U^{1/2}}{3.25(\rho c k)^{1/2}} \tag{16}$$

where $L = R_o U/2\alpha$; α = thermal diffusivity; c = specific heat.

Venogradov et al. [35] made a study of thermal effects by sliding polypropylene disks on metal rings. The conditions were described as heavy duty although the sliding velocity was only 14 cm/sec. Figure 8 shows the coefficient of friction for dry polypropylene as a function of load. The curves have a maximum which was identified with surface melting of the polymer. Increasing load at constant sliding velocity caused an increase in friction. This was attributed to an increase in the contact area. At a critical load the polymer begins to melt, and the friction coefficient decreased with the increasing load. A thin melt layer was found on the surface for the decending branch of each curve. This layer was detected by rapidly cooling the sample and observing the newly formed hard amorphous layer. Test results were grouped into two curves according to the different thermal conductivities of copper and aluminum on the one hand and of steel and cast iron on the other.

McLaren and Tabor [36] presented one of the few studies of polymer friction as a function of typical engineering speed (Figure 9). The results show the distinct maximum coefficient of friction which occurs at a given speed. Although they speculate that the temperature rise was probably of the order of tens of degrees C at less than 100 cm/sec, it is certainly greater at higher speeds.

The friction of nylon against steel was investigated by Cerico [37] with an apparatus that used rotating disks. As the disks rotated at different speeds, a sliding speed of 76 cm/sec was produced in the contact zone. The coefficient of friction required a run-in time before it stabilized (Figure 10). The average roughness decreased with time until it reached 30% of its initial value. As others have

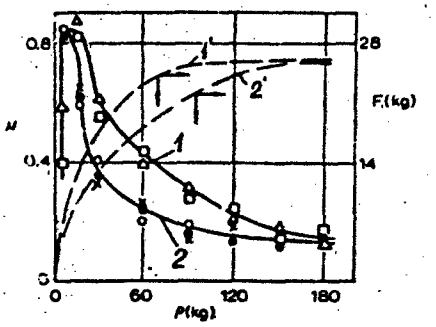

Figure 8. Effect of Load on Dry Metal-to-Polypropylene Friction in Air (Sliding Speed 14.6 cm/sec). 1, copper-aluminum, 2, steel-cast iron

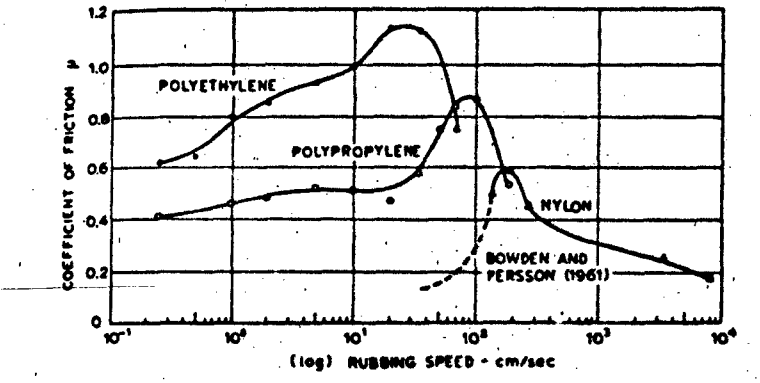

Figure 9. Friction Velocity Dependence of Linear Crystalline Polymers at 22° C. Load 100 g.

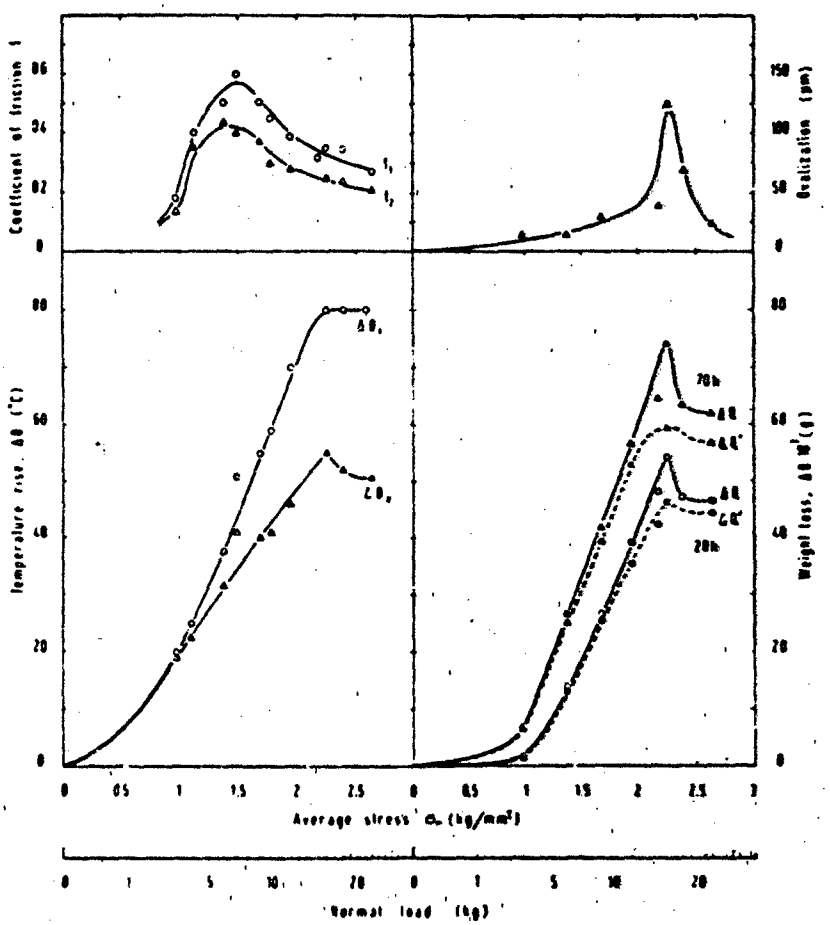

Figure 10. Coefficient of Friction, Ovalization, Temperature Rise, Wear of Nylon ΔQ and Total Wear ΔQ' of Nylon on Steel Pairs vs. Average Stress in Contact Area

observed, an increase in the friction coefficient occurred up to a maximum beyond which a noticable decrease took place. The peak friction coefficient was linked to a significant rise in measured surface temperatures, probably well below the asperity contact temperatures. The friction coefficient decreased with the formation of a layer of nylon on the steel surface. This layer melted for the higher loads. Just recently Clerico [38] reported on friction and wear studies of polyacetals at a sliding speed of 0.45 m/sec. The friction coefficients again displayed a maximum at a load of 50 Newtons and approached an asymptotic value of 0.1 (Figure 11). Wear of the much harder glass filled polyacetal (GV 1/30) was at least 40 times the unfilled material, counter to wear theory. As observed earlier with nylon composites and non-composites [37], the surfaces appeared similar to desert sands which confirmed the presence of polymeric melt. The melted layer solidified into an amorphous brittle layer with a softer sublayer. The thickness of the brittle layer depended on the normal load and sliding distance. For non-composites the layer was about 3-5 μm thick at W = 50 Newtons and about 15 μm thick at W = 200 Newtons. Catastropic wear at high loads and long sliding distances was identified with the disruption of this brittle solidified layer.

Tanaka [39][40] investigated the friction and wear of both glass and carbon filled polyacetal and teflon at sliding speeds up to 2.5 m/sec. Polymer pins (3 mm dia.) were rubbed on both steel and glass disks. It was found that melting of the frictional surface layer occurred easily under ordinary rubbing conditions. The melting depth of the unfilled polyacetal, rubbing against steel, was generally several microns thick while, in the case of a glass disk at higher speeds, it was about twenty microns. For filled polyacetals the melted layer was associated with a very dense fiber rich surface. The carbon filler produced a matted layer over 50 μm thick (Figure 12) while the glass filler formed a mat only near the center of the pin specimen which was attributed to the poorer thermal conductivity of glass.

The coefficient of friction of the filled polymers against glass and steel is shown in Figure 13. The friction coefficient was considerably higher than the values reported by Clerico [38] for

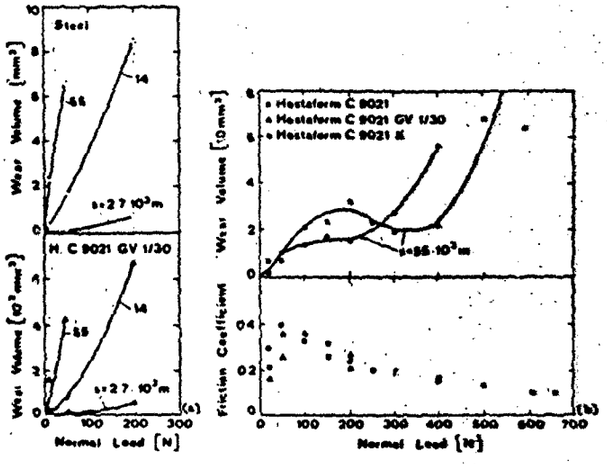

Figure 11. Wear Volume and Friction Coefficient of Plastics vs. Normal Load

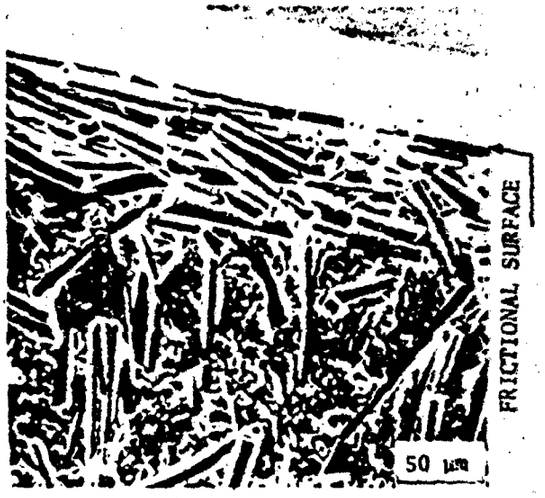

Figure 12. Scanning Electron Micrograph of Carbon Fiber-filled Polyacetal after Rubbing under a Load of 50 N against a Glass Disk at 2.5 m/s

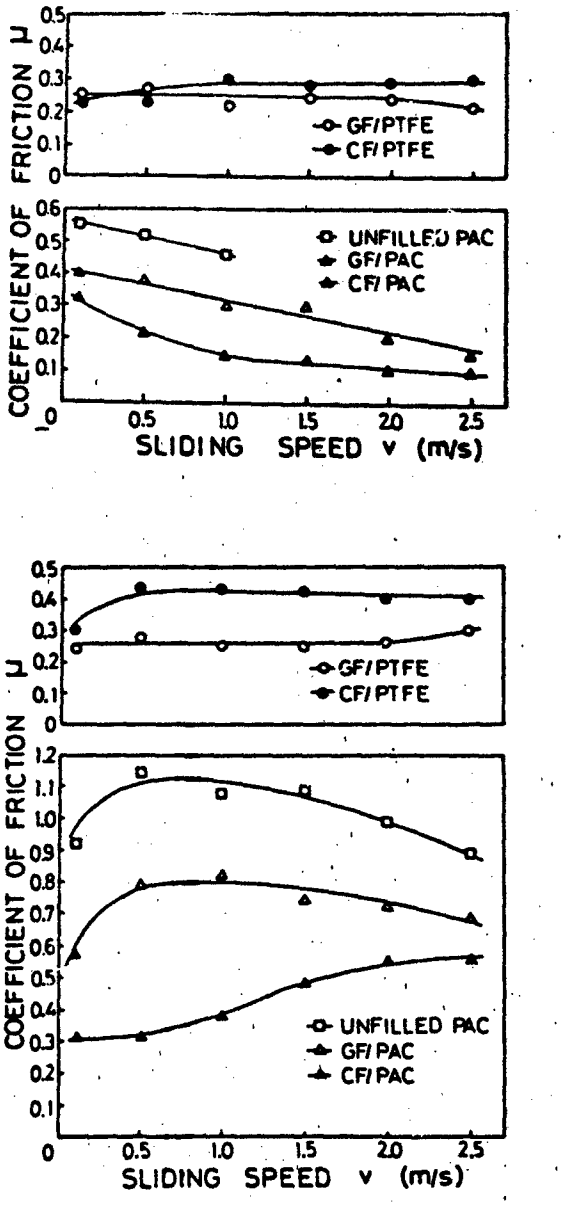

Figure 13. Variations of Coefficient of Friction with Sliding Speed for Various Filled Polymers Rubbed against a Glass Disk (top) and a Steel Disk (bottom)

identical loads and speeds. The difference apparently was due to the contact stress (recall section 3): Tanaka (7 N/mm^2); Clerico (11 to 65); unfilled polyacetal yield strength (73). The fillers promoted lower friction because of the reduced adhesion between fibers and steel. The differences were less pronounced for the glass disk since glass limited heat conduction to the disk and caused melting at lower speeds. In the non-melt region below 0.5 m/sec, the unfilled polyacetal had a much lower wear rate than the filled polyacetal. At higher speeds the filled polyacetals showed marked superiority. Tanaka attributed this behavior to the ability of the fibers to prevent an outflow of molten materials. However, it is also likely that any solidified fiber-filled layer has a much higher strength than the friable, pure, polyacetal layer.

6. POLYMER FRICTION (HIGH SPEED)

Friction at high sliding speeds has been reported in only a few references, preferably with metal to metal contacts, and in each case some evidence or theory has been related to a melt lubrication. The subject was stimulated by World War II in an attempt to understand projectile rotating band friction. Herzfeld and Kosson [41], in a "Confidential" 1953 report recently unclassified, cited military evidence of metal band melt for projectiles reaching speeds up to 6600 ft/sec. They proposed a hydrodynamic slider bearing model of the band riding on its own melt. The melt viscosity was assumed to be constant, and a simple lumped energy balance was used to establish the melt thickness. A feature of their model was the heat loss to the barrel by transient heat conduction. Film thicknesses on the order of 10^{-5} to 10^{-7} cm were predicted.

Wilson [42], unaware of the above work which was not published in the open literature, recently proposed a similar one-dimensional hydrodynamic sliding model for melt lubrication. Again, the fluid temperature was assumed to be constant at the melt temperature and no attempt was made to account for heat transfer from the melt region. However, Wilson did point out that the results differ widely depending on whether the slider melts or its stationary track melts, Figure 14. Bicego, et al. [43] modified Wilson's work to account for heat conduction through the melt film due to a track temperature higher than

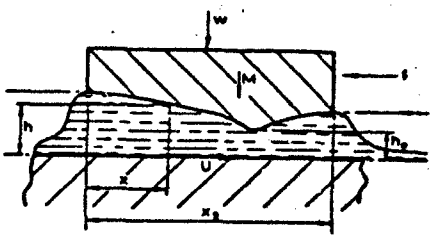

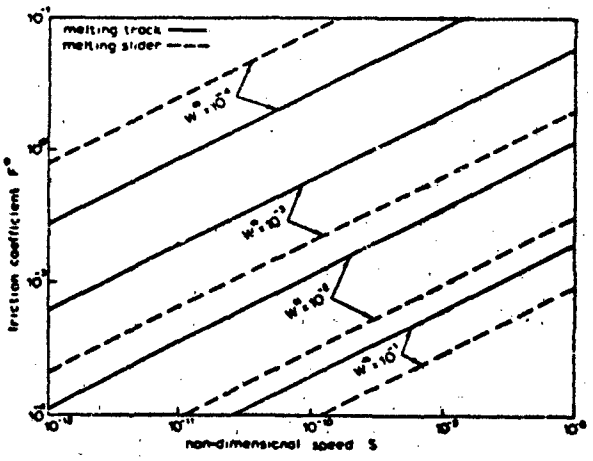

Figure 14. Effect of Load and Speed on Friction

the melting slider. In the case of an ice slider, a small temperature difference (.2°C) was sufficient to make conduction prevail over viscous heating. Results were obtained in terms of the track-slider temperature difference, thus avoiding the actual heat conduction problem.

One of the first published reports on high speed friction was carried out by Johnson, et al. [44]. A steel ball was slid on a steel disk up to speeds of 110 ft/sec. The coefficient of friction decreased from 0.55 to 0.25 for increasing sliding speed. Amontons' law (μ independent of load) was obeyed up to and including loads with contact stresses of 255,000 psi.

Perhaps the most comprehensive experimental study of metal friction and wear at high sliding speeds was done at the Franklin Institute from 1946 to 1956 by Clark, Morsell, and Shugarts. There was no publication of this work in the open literature because it was classified during that time. Montgomery [9] has recently collected all of this data. A pin-disk machine was used to slide various metal specimens against a steel disk. The coefficient of friction decreased with increasing values of pressure x velocity for all tested metals. A typical low coefficient of friction was approximately 0.2. One reported run with a nylon pin gave $\mu = 0.10$ at 900 ft/sec and 4100 psi. Montgomery found that the pin wear rate correlated directly with the reciprocal of the material absolute melting point (Figure 15).

Montgomery [10][11] also reported on experimental work to determine the friction coefficient of projectile rotating bands made from gilding metal (90 CU; 10 Z_N). Measurements of gas propellant pressure, projectile acceleration, and the band normal contact pressure on rounds fired in a 155 mm howitzer were used to calculate the friction coefficient. The results were compared with similar data from the pin-disk experiments of the Franklin Institute (Figure 16). The friction coefficient for rotating bands drops quickly to a steady-state value of 0.02 at a pressure x velocity of approximately 0.8×10^6 (psi)(fps). This value is an order of magnitude below the pin-disk value. Montgomery [11] attributed the difference to the size effect inherent in the hydrodynamic sliding model of melt as proposed by Wilson.

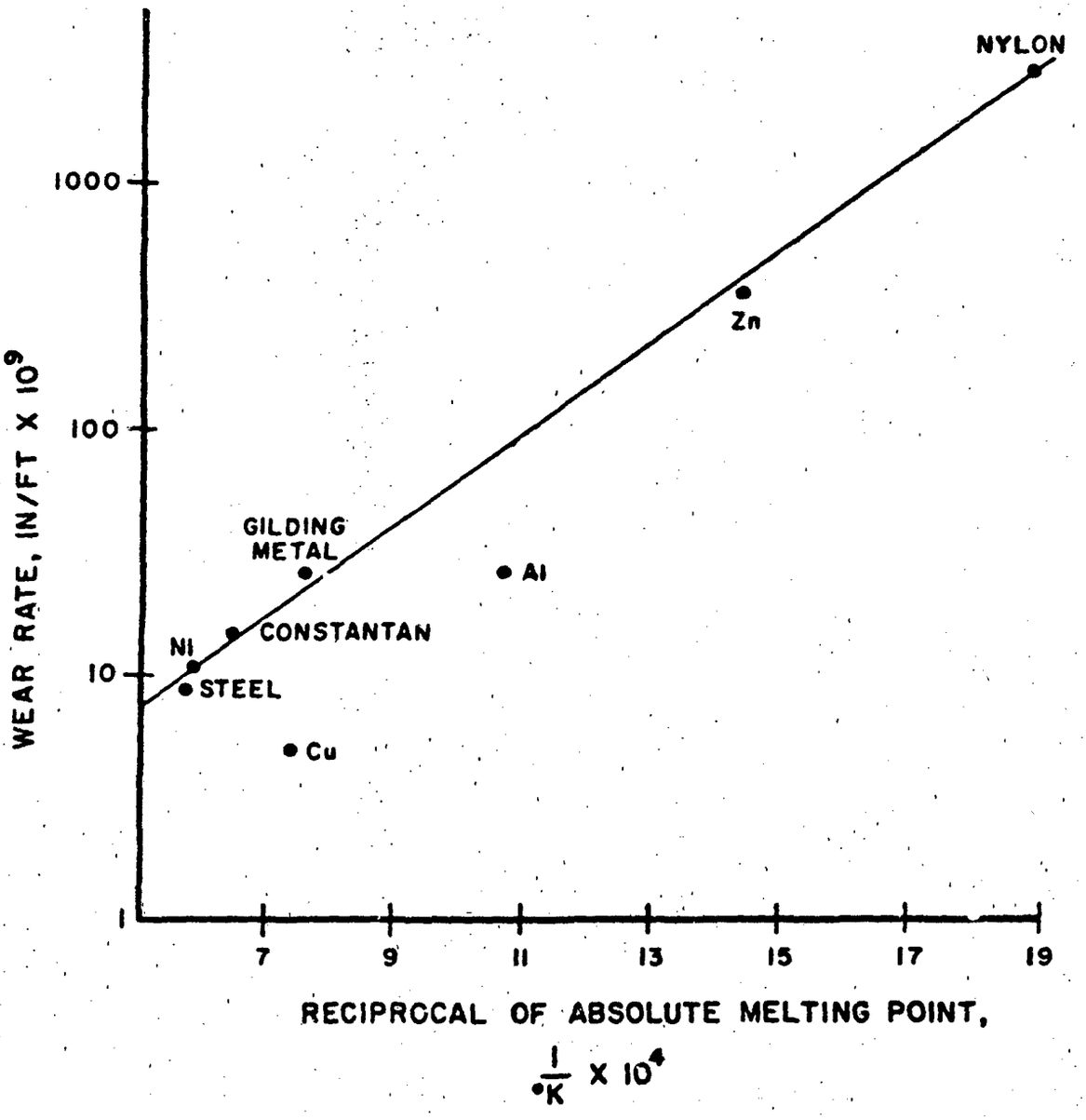

Figure 15. Wear Rates of Different Materials as Function of the Reciprocal of their Absolute Melting Points

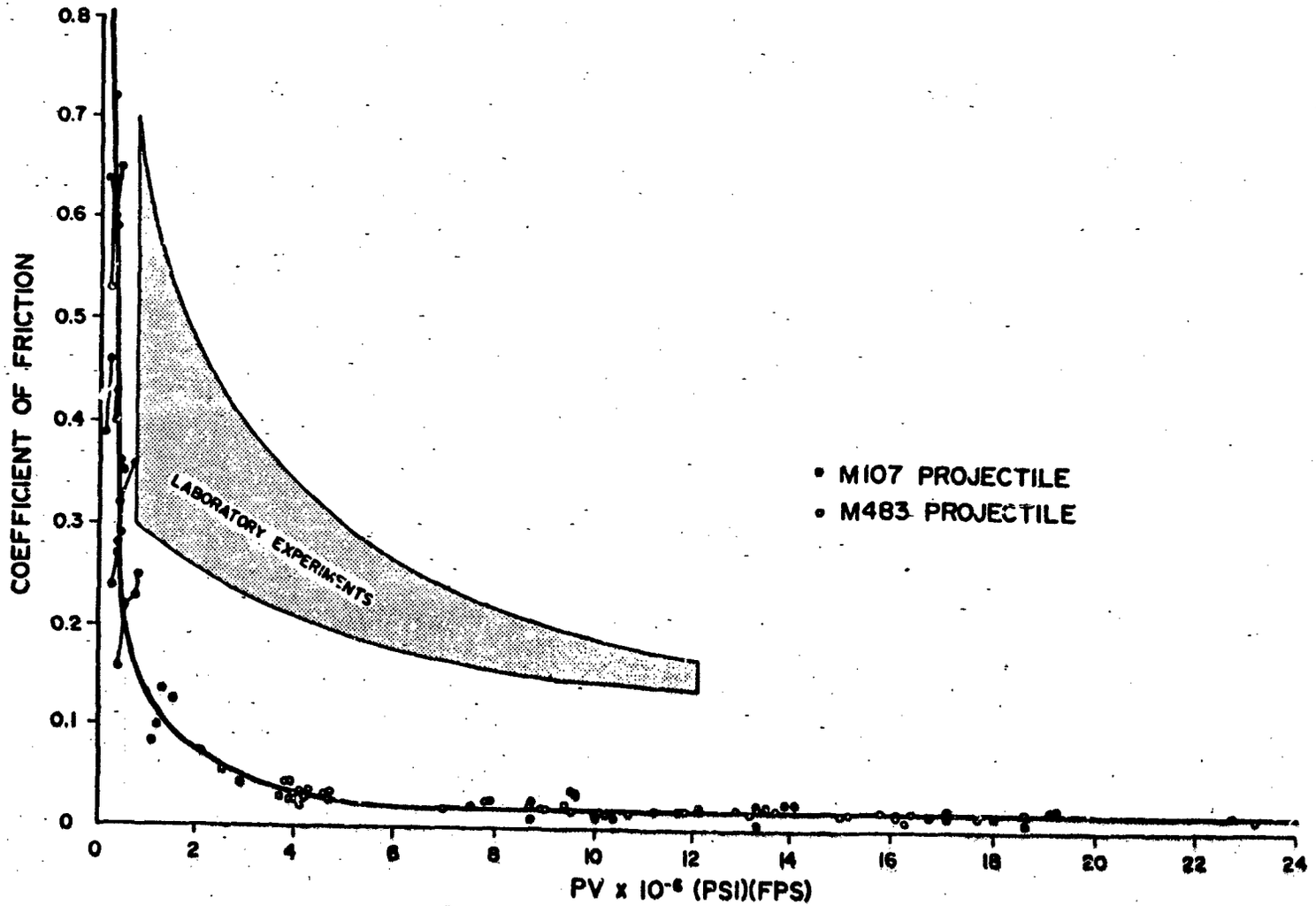

Figure 16. Coefficient of Friction as a Function of the Product of Bearing Pressure and Sliding Velocity for a Projectile with Gilding Metal Rotating Bands

In early experiments using the Franklin Institute pin-disk machine, Sternlicht and Apkarian [45] measured the friction and wear of several metal pins (Mo, W, Cr, Cu, Ag, Al) on a steel disk with speeds up to 2000 ft/sec. Again, the coefficient of friction decreased with an increase in velocity. They measured the electrical contact resistance across the interface of the rubbing metals. An increase in contact resistance with velocity was attributed to the developing molten liquid layer at the interface. In an application of Reynolds' equation to melt lubrication, Sternlicht and Apkarian proposed the thermal wedge [46] (increasing film temperature gradient in the direction of motion) as the mechanism to support a normal force between parallel surfaces moving with relative velocity. Based on the solution of this problem, the investigators found that the calculated pin wear, due to end leakage of the molten film, differed from the measured wear within an order of 100%. Neither the basic equations nor the solution details were offered in the paper.

Bowden and Freitag [47] studied high speed friction by spinning a steel ball in a magnetic field and measuring the deceleration when it was brought in contact with a metal or diamond surface. Melting occurred at the region of contact. An analysis of the heat flow into the specimen showed that the area of intimate contact was very small compared to the apparent area.

Bowden and Persson [48] continued the spinning ball experiments of Bowden and Freitag and presented an in-depth study of melt with high speed friction. Figure 17 shows the results with a 5-kg load for a steel ball sliding on Woods alloy (m.p. 65°C), bismuth (m.p. 271°C), tin (m.p. 232°C) , lead (m.p. 328°C), copper (m.p. 1080°C) and steel (m.p. 1500°C). Minimum coefficients of friction shifted to higher sliding velocities as the metal melting point increased. In several cases the minimum coefficient of friction was well below a value of 0.1. A substantial increase in wear occurred at sliding velocities corresponding to the minimum μ. Examination of worn surfaces revealed large formations of splashed-out solidified material near the leading edge as well as small globules of solidified melt on the wear track. This evidence was much less pronounced on the high melting copper and steel. Using the work of Landau [49], who determined the propagation

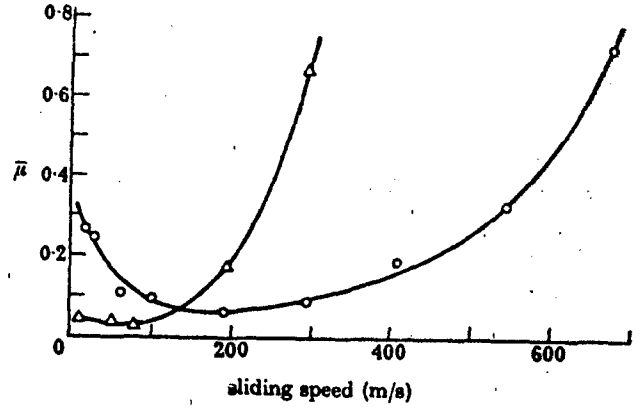

Steel sliding on Wood's alloy (Δ) and bismuth (O).

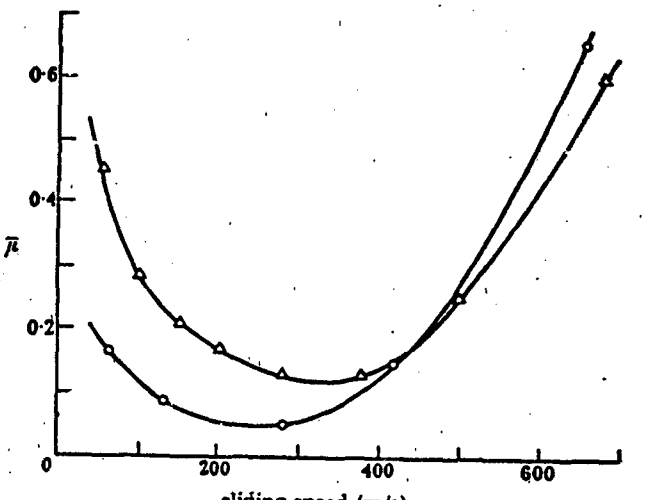

Steel sliding on lead (Δ) and tin (O).

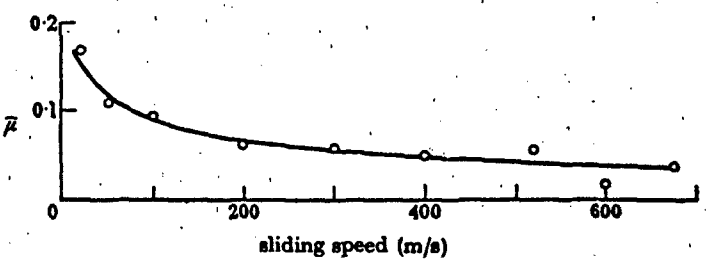

Steel sliding on itself.

Figure 17. High Speed Effects on Sliding Friction (metals)

of a melt-solid interface, Bowden and Persson crudely calculated the time for a steady state melt condition to be reached, approximately 10^{-5} sec. This number was much smaller than the ball contact time. Figure 18 shows the results for several non-metals: silver nitrate (m.p. 210°C), nylon (m.p. 265°C), teflon (decomposes at 400°C), butadiene styrene copolymer rubber, and glass (m.p. 800°C). Both silver nitrate and glass developed the typical wall of molten material at the leaving edge. Teflon displayed a rough hide-like texture at high speeds denoting uneven decomposition. Molten nylon was splashed out of the wear mark; however, the surface had a large number of pits or dimples, and the extruded material contained bubbles, suggesting gaseous matter was produced. The rubber also had a foamy appearance to the molten debris. Another approximate calculation by Bowden and Persson indicated that steep temperature gradients existed across the molten nylon film with film temperatures exceeding 800°C. Metal film temperatures probably were only a few degrees above the melting temperature even at the higher speeds. This difference was attributed to large melt viscosities and low thermal conductivities of polymers.

Miller [50] investigated the surface of various carbides and oxides with high melting points after they were subjected to the same spinning steel ball apparatus as above. Wear from a network of surface cracks correlated with their lack of resistance to thermal shock.

Carignan and Robinowicz [51] have carried out sliding tests of soft metal and nonmetal pins on a rotating steel disk at speeds up to 150 m/sec. The friction data was in approximate agreement with those obtained by others using the pin-disk geometry.

7. DISCUSSION

A review of the literature indicates the following scenerio for the effect of sliding velocity on the coefficient of friction. For low sliding velocities the coefficient of friction increases with speed, presumably caused by an increased contact area. At some critical velocity, on the order of several feet per second for polymers, the friction coefficient peaks and begins to decay with increasing speed. Evidence is overwhelming that material melting occurs at the asperity tips for these relatively low sliding velocities. Melting increases

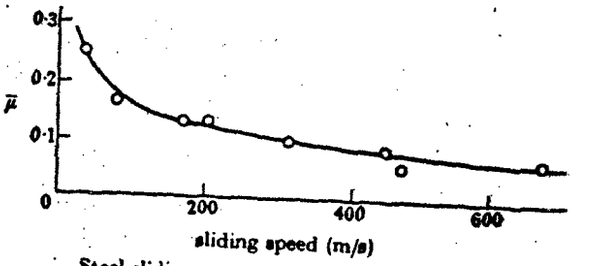

Steel sliding on nylon. $\bar{\mu}$ as a function of sliding speed.

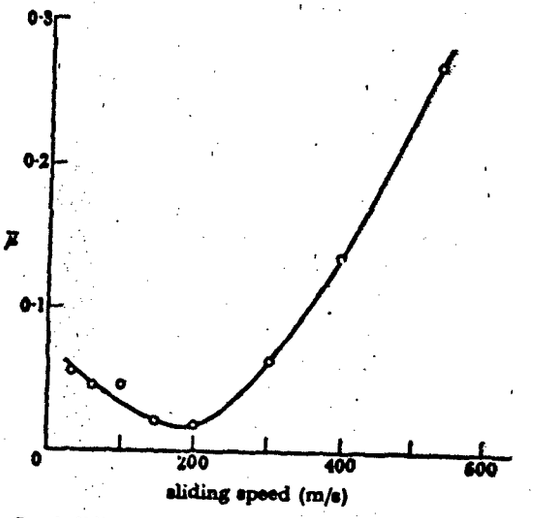

Steel sliding on silver nitrate.

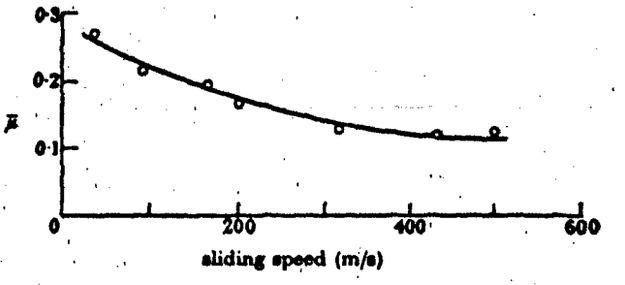

Steel sliding on *PTFE*.

Figure 18. High Speed Effects on Sliding Friction (Non-Metals)

with sliding speed until the entire apparent contact area is a layer of melted material. The speed at which the full melt layer exists is not established, but it does depend on the load. The data from several sources suggest that several hundred feet per second is sufficient for a full melt of polymer material at light loads (pressures much less than the yield stress). Although several authors in the early 70's discussed the importance of apparent pressure as a parameter in friction work with polymers, load continues to be used instead. Little work was done at high loads with the exception of internal ballistics. Montgomery found that silding metal produced a full melt layer at PV = 5×10^6 (psi)(fps). For measured contact stresses of 50,000 psi, this limit gives a sliding velocity of 100 ft/sec. Polymers have much lower thermal conductivities and melting points than metals.

Two recent references [42][43] focused on a melt lubrication model to explain the low friction of ice. This model relied on the hydrodynamic slider bearing concept. Montgomery noted that the coefficient of friction for gilding metal from internal ballistics (μ = 0.02) tests was much lower than values found for pin-disk experiments ($\mu > 0.1$). It is significant that most experimental work on friction was accomplished with pin-disk machines, all pin diameters being nearly 1/10 inch. All reported coefficients of friction on these machines were greater than 0.1 at high speeds. The one exception was the work done by Bowden and Persson [48] on spinning steel balls. Here, friction coefficients well below 0.1 were recorded.

One difficulty with the slider bearing concept is the need for a lubricant at the front edge of the slider. Wilson [42] was well aware of this problem and he recommended a minimum load before melt lubrication can occur. Montgomery seized upon the length factor of this minimum load to explain the difference in friction coefficients between sliding projectile bands and pin-disk experiments at comparable conditions. This writer will propose an alternate solution to the melt lubrication problem below which circumvents the lubricant problem; however, there is a better explanation for the high friction coefficients achieved with pin-disk experiments. If the friction coefficient is calculated from slider bearing theory [46], it's value

is proportional to a functional of the length to width ratio which characterizes rotating bands, when compared to the ratio of one for pins.

(The reverse of this page is blank.)

SECTION III

LITERATURE REVIEW OF RHEOLOGY

1. NEWTONIAN BEHAVIOR (OILS)

For Newtonian fluids the shear stress is linearly related to the strain rate, i.e.,

$$\tau = \mu \frac{du}{dy} \tag{17}$$

The absolute viscosity μ is generally dependent on pressure and temperature. Early measurements made at Harvard and sponsored by ASME [52] show this dependency over a large range. They suggested an empirical relationship

$$\ell n\left(\frac{\mu}{\mu_o}\right) = c\, e^{\beta/T}\left\{1 + \alpha p - B[\alpha p - e^{-\alpha p})]\right\} \tag{18}$$

The constants μ_o, c, B, α, β vary for each oil.

At atmospheric pressure the variation of viscosity with temperature is given by

$$\ell n\left(\frac{\mu}{\mu_o}\right) = c\, e^{\beta/T} \tag{19}$$

The relationship between temperature and either Saybolt seconds or kinematic viscosity may be plotted as a straight line on charts with special scales, known as the ASTM Standard Viscosity Temperature Charts for Liquid Petroleum Products D341. However, straight lines for absolute (dynamic) viscosity may be plotted with minor error as shown in Figure 19.

In most hydrodynamic theory the effect of pressure is not taken into account. This effect can be ignored up to a fluid pressure of 1000 psi, but at pressures of 5000 psi ordinary lubricating oils double their viscosity. In 1893 Barus established an empirical equation to describe isothermal viscosity-pressure relationship for a given liquid:

$$\frac{\mu}{\mu_o} = e^{\alpha p} \tag{20}$$

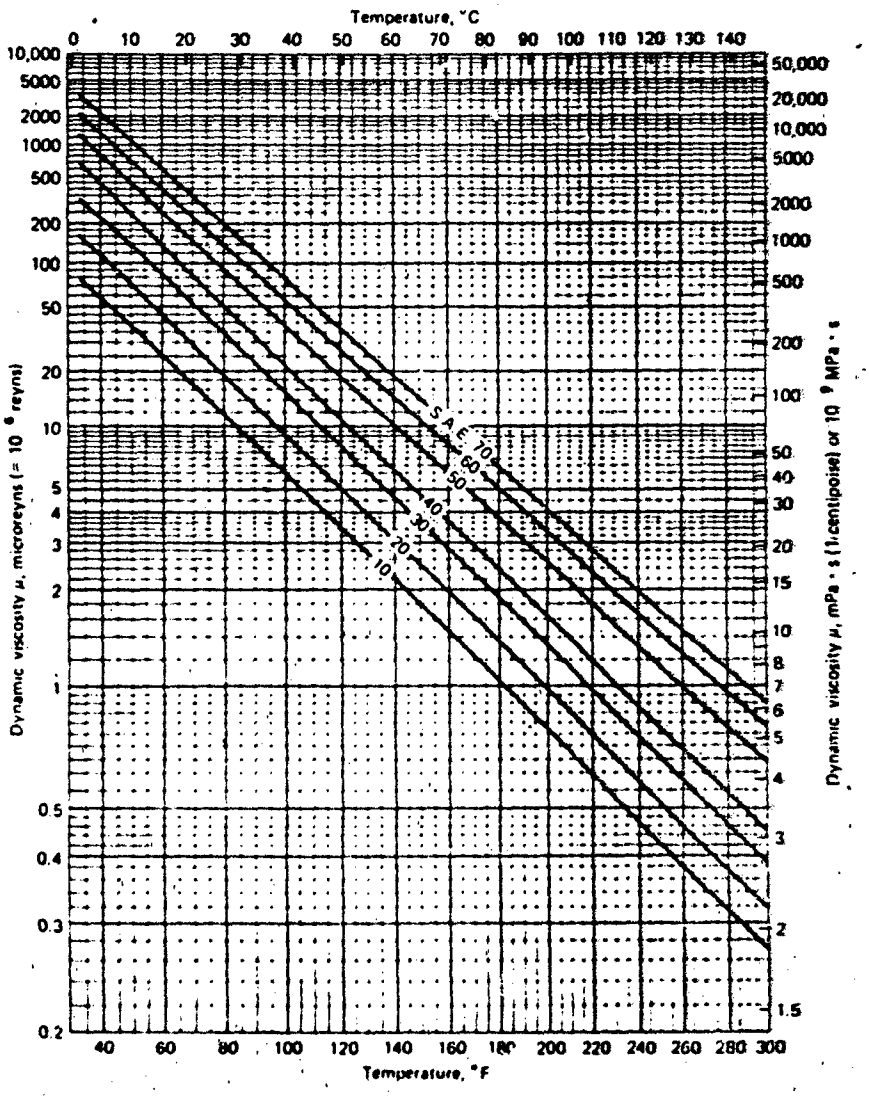

Figure 19. Dynamic or Absolute Viscosity vs. Temperature for SAE-Numbered Oil

Eyring and co-workers [53] have derived a similar relationship based upon molecular free volume mobility theory. Generally $1/\alpha$ is approximately equal to 7000 psi for most mineral oils, resins, and polymer blends. An early summary on pressure-viscosity work was published by ASME [54], see Figure 20.

Interest in viscosity-pressure correlations has paralleled interest in elastohydrodynamics (EHD). Equation (20) above overestimates the viscosity at very high pressures. Cameron [55] has proposed

$$\frac{\mu}{\mu_o} = (1 + Cp)^n \qquad (21)$$

Other correlations are discussed by So and Klaus [56] and Johnson [57]. Allen, C. W., et al. [58] reported that spinning ball experiments showed poor agreement between load and torque using equation (20). They proposed a modified exponential form (Figure 21):

$$\frac{\mu}{\mu_o} = e^{\alpha p} \qquad p \leq p_m$$

$$= e^{\alpha p_m} + \beta(p - p_m) \qquad p > p_m \qquad (22)$$

A similar model was used successfully by Cheng [59]. However, Johnson [60] argues that the reduced viscosity at very high pressures is caused by the shear stress limiting feature of the oil at these pressures. Non-Newtonian fluid behavior is now discussed.

2. NON-NEWTONIAN BEHAVIOR (OILS)

Non-Newtonian fluid behavior is characterized by a viscosity which varies with rate of shear. Polymer-thickened oils (oils containing VI improvers) usually suffer viscosity losses when subjected to high shear rates. These losses can be either permanent (due to a mechanical or chemical breakdown of the larger molecules) over a period of time, or it can be temporary, recovering the original viscosity when the stress is removed. We are concerned with the latter.

The American Petroleum Institute (API) in conjunction with the ASTM conducted an investigation on viscosity variation with shear rates, reported in ASTM Special Technical Publication No. 111: "Symposium on Methods of Measuring Viscosity at High Rates of Shear."

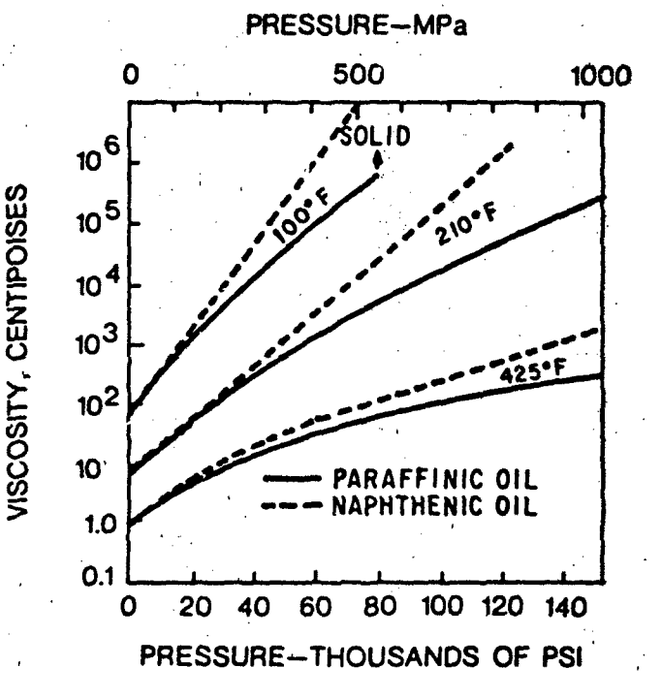

Figure 20. Viscosity-Pressure Relationships for Paraffinic and Naphthenic Oils at Three Temperatures

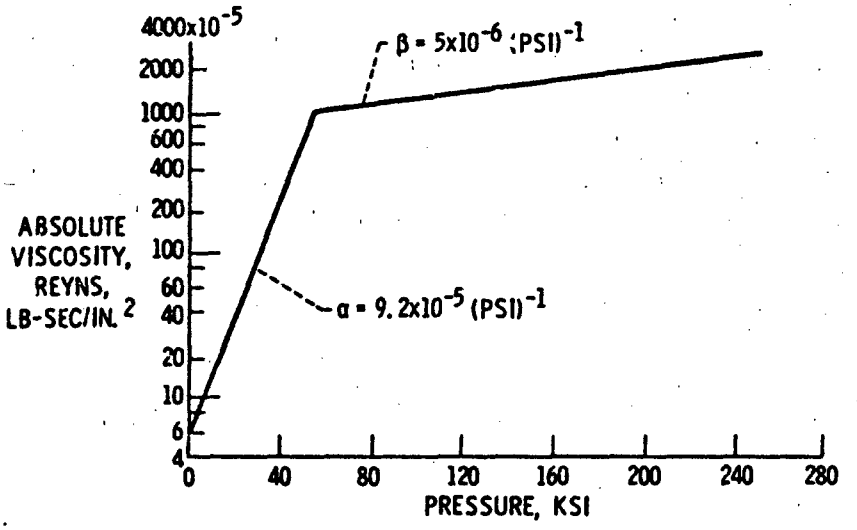

Figure 21. Theoretical Pressure-Viscosity Relation for Synthetic Paraffinic Oil at 83°F

Two polymer blended oils underwent a 30-40 percent temporary viscosity loss at shear rates of 50,000 to 1,000,000 sec^{-1}--comparable to rates found in automobile engines. Klaus and Fenske [61] reported on viscosity-shear characteristics of lubricants and related the results to hydraulic systems. West and Selby [62] studied the effect of multigraded polymer blended engine oils and found permanent viscosity losses. In January of 1964, a symposium was held by ASTM and published in ASTM Special Technical Publication No. 382: "The Effects of Polymer Degradation on Flow Properties of Fluids and Lubricants Containing Polymers."

In the mathematical description of non-Newtonian fluids it is necessary to retain the basic momentum equation in lubrication:

$$\frac{\partial p}{\partial x} = \frac{\partial \tau}{\partial y} \tag{23}$$

Flow properties of the lubricant are expressed in one of two general forms:

$$\frac{\partial u}{\partial y} = F_1(\tau) \tag{24}$$

or the inverse

$$\tau = F_2(\partial u/\partial y) \tag{25}$$

Greases have been modeled as Bingham plastics by Milne [63][64]:

$$\tau = \pm\tau_o + \mu \frac{\partial u}{\partial y} \tag{26}$$

in which a yield value must be reached before flow takes place. Examples can be found in Pinkus and Sternlicht [65]. If a liquid is stressed rapidly enough, it will display an elastic response to stress; thus, the duration of the stress becomes a parameter in describing the properties of such fluids. Milne [66] has applied a Maxwell model of a lubricant (linear viscoelastic fluid) to the theoretical treatment of slider bearings:

$$\frac{\partial u}{\partial y} = \frac{1}{G}\frac{d\tau}{dt} + \frac{\tau}{\mu} \tag{27}$$

were G is the elastic modulus and the viscous dissipation term (second on right) is Newtonian. If conditions are steady, the time derivative may be replaced by the space derivative and

$$\frac{\partial u}{\partial y} = \frac{U}{G}\frac{\partial \tau}{\partial x} + \frac{\tau}{\mu} \qquad (28)$$

Non-Newtonian effects can also be expressed in terms of non-linear viscous dissipation and/or shear limiting effects. Smith [67] was the first to suggest that lubricants under high pressure contacts display characteristics that are solid-like. Johnson and Cameron [68] carried out experiments using cylindrical disks in combined rolling and sliding for high contact pressures. They reported curves similar to Figure 21; however, Johnson [60] speculated that the lubricant behaved as a granular solid, displaying a critical shear stress which can not be exceeded, rather than possessing a reduced viscosity at the high pressures.

a. Glass Transition

When lubricants are cooled, they do not solidify into a crystalline solid at some fixed temperature. Instead their viscosity steadily increases until the material exhibits a solid-like behavior referred to as a glass (amorphous ductile solid). Although the process is continuous, properties such as specific volume or speed of sound show a marked change at the glass transition temperature. The glass transition temperature is not fixed. Since the transition is a viscoelastic phenomenon, it responds in a glassy (elastic) way at ambient pressures and temperatures as in the early ASTM work above. A major method to test the viscoelasticity of oils to strain rates is the use of oscillatory shear at frequencies to 78 MHz. The now classic paper in this field is that of Barlow and Lamb [69]. Major contributions have been made by Dyson [70][71] to incorporate the above work into a continuous shear mechanism of EHD. Differences between oscillatory shear and EHD experiments to extract the elastic shear modulus is attributed to relaxation times by Johnson [72]. A good summary of the oscillatory shear approach to rheology is given by Hutton [73].

Hirst and Moore [74] have shown that a viscosity in the EHD contact region of 10^5 p_a-s (14.5 lb-sec/in^2) is a good working criterion for the onset of an elastic response. If the glass transition is a consequence of the viscosity reaching a critical value, the transition could equally as well be brought about by increasing the pressure isothermally as by cooling at constant pressure. Johnson and Roberts [75] revealed viscoelastic behavior in a point contact disk machine at contact pressures greater than 0.5 Gp_a (72,500 psi). Sliding speed (strain rate) was very low. This aspect of glass transition has been studied by Alsaad, et al. [76]. They observed that glassy states are very likely for most lubricants in EHD contacts and occur at lower pressures for sliding as opposed to rolling contacts. Also, the glass transition temperature rises with increasing pressure, Figure 22.

b. Johnson Rheology Model

The impetus for viscoelastic studies of lubricants in EHD contacts was the traction problem using disk machines (two parallel rollers with different peripheral speeds. Typical traction curves [77] are shown in Figure 23. In general there are three regions: (i) a linear Newtonian region, (ii) a non-linear region where the traction approaches a constant value independent of the rate of shear (slip), and (iii) a thermal region. The traction is dominated by the non-linear region. Hirst and Moore [78] first presented a <u>non-linear</u> viscous flow model for high pressure EHD based upon the Eyring thermal activation theory. Expanding on this idea Johnson and Tevaarwerk [79] developed a non-linear Maxwell model described by

$$\frac{du}{dy} = \frac{1}{G}\frac{d\tau}{dt} + F(\tau) \qquad (29)$$

where

$$F(\tau) = \frac{\tau_o}{\mu}\sinh(\tau/\tau_o) \qquad (30)$$

and τ_o is an experimental constant. At small shear stresses $F(\tau)$ reduces to τ/μ--a Newtonian fluid. It is important to realize that G and τ_o depend upon temperature and pressure as does the viscosity. The

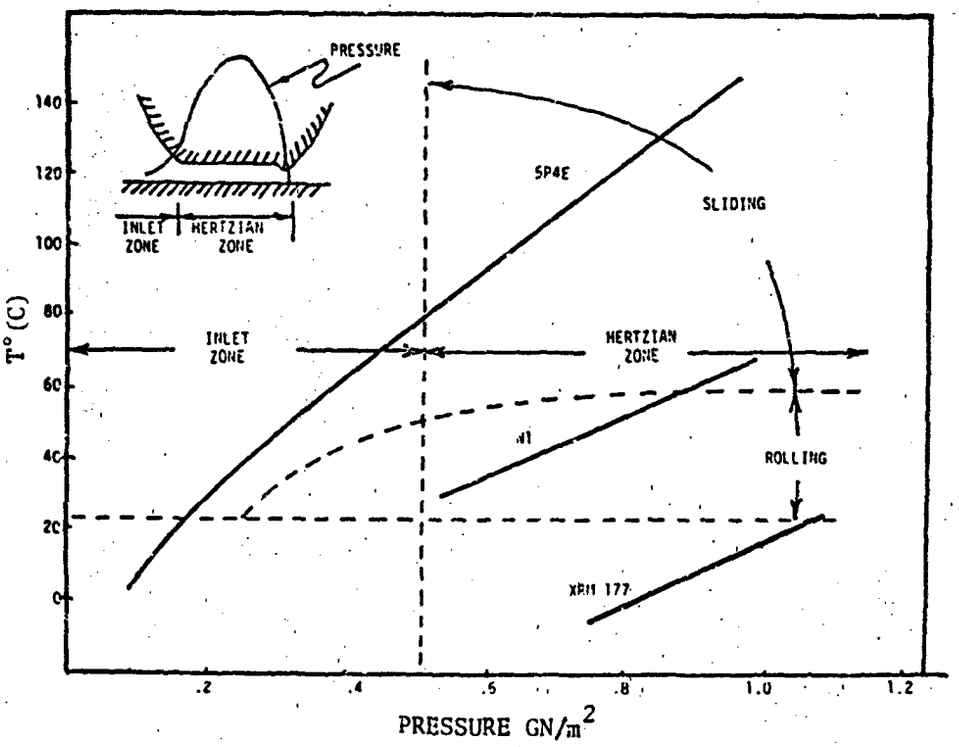

Figure 22. Heuristic Estimates of the Relationship Between Conditions in an EHD Contact and Glass-Liquid Phase Diagrams of Some Lubricants

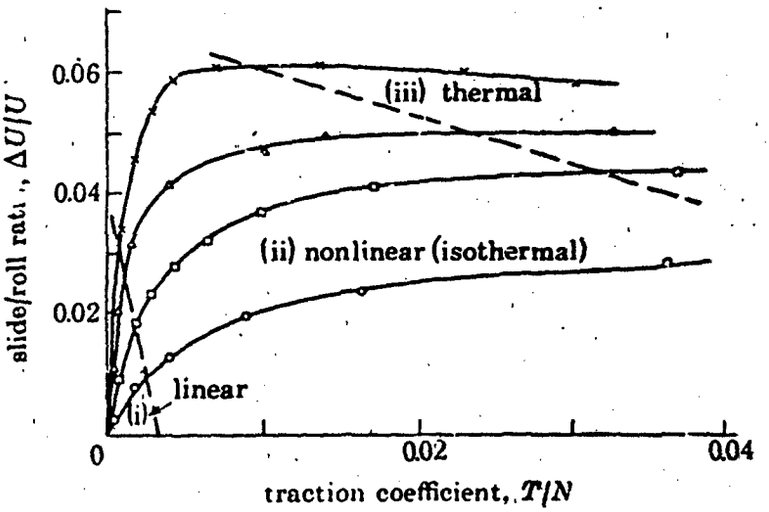

Figure 23. Typical Traction Curves Measured on a Two-Disk Machine in Line Contact at Varying Mean Contact Pressures

success of this model is shown in Figure 24 which includes data from a disk machine. The dimensionless number D (Deborah number) = μU/Gb where b is the contact radius.

Eyring's equation for non-linear shear rates may be written

$$\frac{du}{dy} = A \exp\left[-\frac{v_1 p+E}{kT} \sinh \frac{v_2 \tau}{kT}\right] \qquad (31)$$

where A is a constant, E is the activation energy at atmospheric pressure, T is the absolute temperature, k is the Boltzmann's constant, v_1 and v_2 are activation volumes for pressure and shear, respectively. When $v_{2\tau} >> kT$

$$\frac{du}{dy} = \frac{1}{2} A \exp \frac{v_2\tau - v_1 p - E}{kT} \qquad (32)$$

or comparing with equation (30)

$$\tau_o = kT/v_2$$

$$\mu = \frac{2kT}{v_2 A} \exp\left[\frac{v_1 p+E}{kT}\right]$$

In the high strain rate region equation (32) implies that, at constant strain rate,

$$\tau = \left(\frac{v_1}{v_2}\right) p + \text{constant} \qquad (33)$$

Such a relationship has been recently found for the shear of solid amorphous polymers [80][81][82][83][84].

c. Winer Rheology Model

Experiments have been undertaken by Bair and Winer [85] to measure the shear stress versus shear rates (low rates 10^{-4} s^{-1} to high rates 10^2 s^{-1}) for various lubricants under high pressure contacts, see Figure 25 for example. The data lies primarily in the high shear region which exemplifies the limiting shear stress. This data is compatible with Johnson above who acknowledged a limiting shear stress by advocating a Prandtl-Reuss model, (elastic-plastic solid) at very high rates of strain. Bair and Winer were able to collapse the data for several lubricants by means of the non-linear viscous model

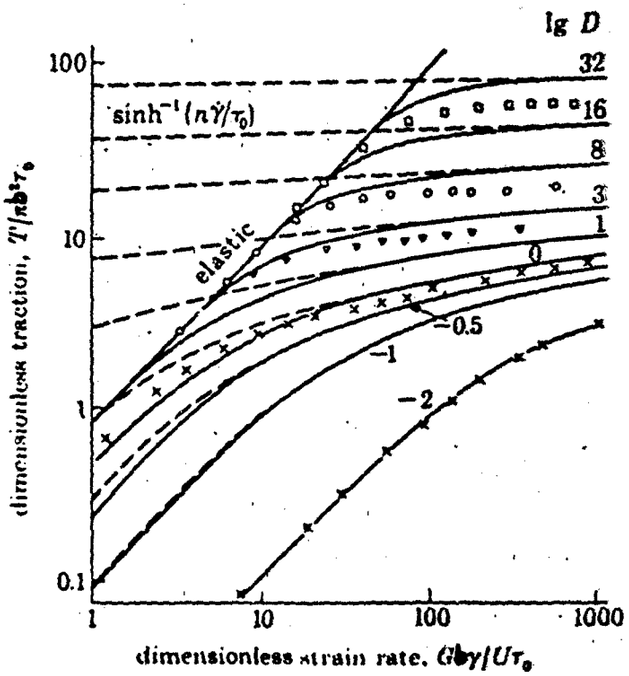

Figure 24. Theoretical Non-Dimensional Traction Curves for Varying Deborah Number

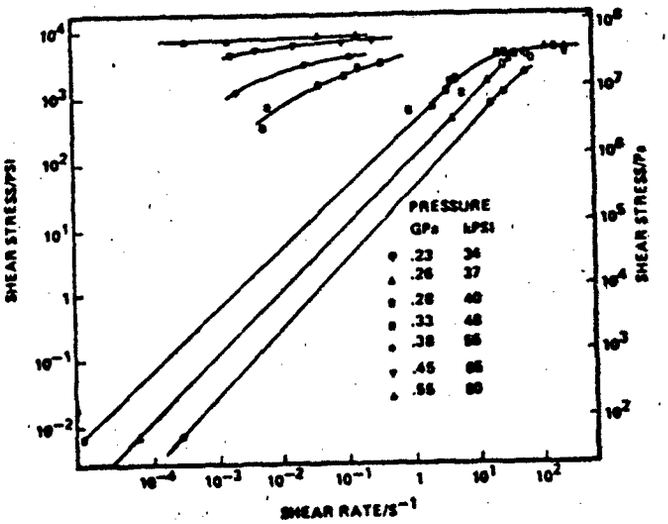

Figure 25. Shear Stress-Shear Strain Rate of 5P4E at 40°C and Indicated Pressure

$$F(\tau) = -\frac{\tau_L}{\mu} \ln\left(1 - \frac{\tau}{\tau_L}\right) \qquad (34)$$

where τ_L is the limiting shear stress. Again τ_L depends on pressure and temperature. Recent experimental data by Bair and Winer [86] for twelve lubricants give pressure and temperature effects on viscosity, elastic modulus, and the limiting shear stress. See also Houpert, et al. [87].

3. POLYMERS

Oils under the extreme pressures of elastohydrodynamic (EHD) contacts thicken to the point of becoming plastic-like. Thus, their behavior is very similar to polymer melts. The viscosity of polymers have been described by expirical relations for over a half of a century while the description of oils under EHD contacts is very recent. Polymer rheology is now reviewed.

Eyrings theory [88], outlined for oils in Section 2b., was proposed to explain the shear behavior of polymers as early as 1936. Let the shear rate $du/dy \equiv \gamma$. Then rearranging equation (31)

$$\mu = \frac{\tau}{\dot{\gamma}} = \frac{\tau}{A \exp\left[(a_1 P/T)+(a_2/T)\right] \sinh(a_3\tau/T)} \qquad (35)$$

If temperature changes are not too large when pressure and shear stress changes occur,

$$\mu = f_1(M) f_2(T) f_3(P),\ f_4(\tau) \qquad (36)$$

where M is the molecular weight. It has been found experimentally that most unbranched linear polymers having a molecular weight in excess of the critical M_c obey the above rule of logarithmic additivity of viscosity. A linear polymer is a polymer in which the molecules are linked together in the form of chains with little side links or branches such as high density polyethylene.

At low shear stress (or shear rates) equation (35) becomes Newtonian but with increasing shear stress the polymer melt viscosity decreases in a characteristic way, giving rise to what is known as a non-Newtonian flow. A number of empirical equations have been proposed to describe this behavior. The best known is the power law model of Ostwald-de Waele (1923):

$$\tau = c\dot{\gamma}^N \tag{37}$$

Figure 26 illustrates this law very well [89]. Thus,

$$\mu = c\dot{\gamma}^{N-1} \tag{38}$$

or

$$\mu = c'\tau^{(N-1)/N} \tag{39}$$

where N is called the "flow index" of the polymer. From equations (38) and (39) it is not surprising that the shear stress functional is often replaced by a shear rate functional in equation (36) for linear polymers.

Of course the power law can not adequately represent the non-Newtonian flow behavior over a wide shear rate range nor can it predict the transition to the low-shear limiting Newtonian viscosity. Mendelson [90] proposed the following for a good fit to experimental data at low shear rates:

$$\log \tau = C_o + C_1 \log \dot{\gamma} + C_2(\log \dot{\gamma})^2 \tag{40}$$

Parrini et al. [91] investigated the melt rheology of nylon - 6, nylon - 6, 10, and nylon - 11 by different techniques and arrived at the following relationship:

$$\log \tau = -2.88 + 2.18 \log(\mu_o\dot{\gamma}) - 0.121[\log(\mu_o\dot{\gamma})]^2 \tag{41}$$

which is valid for shear stresses upto 1500 psi. A recent correlation by Mount and Chung [92], which includes temperature, is shown in Table 1 for several polymers.

Recognizing the limiting viscosity at high shear rates Cross [93] proposed a semiempirical relationship:

$$\mu = \mu_\infty + \frac{\mu_o - \mu_\infty}{1 + (\lambda\dot{\gamma})^m} \tag{42}$$

where λ is a temperature dependent constant and

$$m = (\bar{M}_N/\bar{M}_N)^{0.2}$$

However, the relationship is a four-parameter (unknown) equation. Other empirical relations include

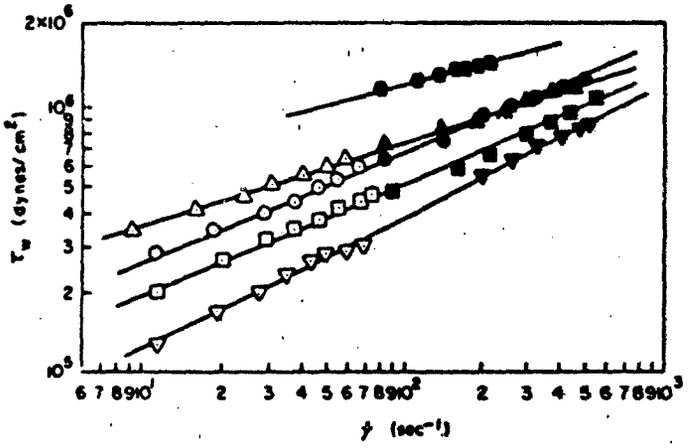

Shear stress versus shear rate for polymer melts at 200°C (31). Closed symbols for capillary die data, and open symbols for slit die data: (●) polymethylmethacrylate; (△, ▲) polystyrene; (⊙, ◉) high-density polyethylene; (□, ■) polypropylene; (▽, ▼) low-density polyethylene.

Figure 26. Shear Stress vs. Shear Rate for Polymer Melts

TABLE 1. PHYSICAL PROPERTY DATA OF POLYMERS USED IN COMPUTER SIMULATION

	Polymer/Source						
	HDPE	LDPE	PP	POM	PS	PMMA	PC
	Phillips Petroleum	Exxon Chemical	Exxon Chemical	Celanese Chemical	Foster Grant	Rohm and Haas	General Electric
Viscosity const.	$(\ln \eta = C0 + C1 \cdot \ln \dot{\gamma} + C11 \cdot (\ln \dot{\gamma})^2 + C12 \cdot T \cdot \ln \dot{\gamma} + C2 \cdot T + C22 \cdot T^2$; η in poise, T in °C, $\dot{\gamma}$ in sec^{-1})						
C0	12.4467	15.7819	13.4196	15.0145	22.7143	17.4067	27.1603
C1	-4.48624×10^{-1}	-7.10087×10^{-1}	-5.39323×10^{-1}	-3.62768×10^{-1}	-9.70531×10^{-1}	−1.63466	0
C11	-1.02613×10^{-2}	-1.57821×10^{-2}	-2.22961×10^{-2}	-5.08060×10^{-2}	-2.46374×10^{-2}	-2.94447×10^{-2}	0
C12	4.00046×10^{-4}	1.68650×10^{-3}	8.59297×10^{-4}	2.21335×10^{-3}	2.81530×10^{-3}	6.56006×10^{-3}	0
C2	-1.07322×10^{-2}	-3.21927×10^{-2}	-1.16103×10^{-2}	-2.87476×10^{-3}	-7.22479×10^{-2}	1.58260×10^{-2}	-9.03876×10^{-2}
C22	3.57691×10^{-6}	2.85122×10^{-5}	-6.75450×10^{-6}	1.99446×10^{-5}	8.22414×10^{-5}	-2.03489×10^{-4}	8.674×10^{-5}
ρ_s, gm/cm³	0.963	0.92	0.897	1.41	1.0	1.19	1.2
ρ_m, gm/cm³	0.777	0.777	0.76	1.16	0.978	1.11	1.1
C_m, cal/gm °C	0.55	0.66	0.48	0.33	0.29	0.33	0.34
k_m, cal/cm °C s	5.79×10^{-4}	4.34×10^{-4}	4.34×10^{-4}	6.41×10^{-4}	6.201×10^{-4}	4.55×10^{-4}	6.3×10^{-4}
T_m, °C	132.0	110.0	165.0	166.0	—	—	—
T_c, °C	—	—	—	—	100.0	105.0	150.0
λ, cal/gm	44.0	31.0	31.9	43.7	—	—	—
ΔH_f, cal/gm	—	—	—	—	26.6	29.4	42.5
[MI]	3.5	2.9	—	2.5	—	2.0	—
[MF]	—	—	5.2	—	—	—	—

Bueche and Harding [94]

$$\frac{\mu}{\mu_o} = [1 + 0.6(\lambda\dot{\gamma})^{0.75}]^{-1} \tag{43}$$

where $\lambda = 12\mu_o M/\pi^2 \rho kT$ (44)

Vinogradov [95]

$$\frac{\mu}{\mu_o} = \left[1 + 0.4\left(\frac{\mu_o\dot{\gamma}}{C}\right)^{0.355} + \left(\frac{\mu_o\dot{\gamma}}{C}\right)^{0.71}\right]^{-1} \tag{45}$$

where $C = 1.9$ psi

Graessley [96]

$$\frac{\mu}{\mu_o} = \left[1 + 1.916(\tau_o\dot{\gamma}/2)^{0.808}\right]^{-1} \tag{46}$$

The above empirical fits do not include the high shear rate asyptotes. However, considering the denominator powers of the shear rate are approaching one,

$$\tau_\infty = \mu_\infty\dot{\gamma}_\infty = \mu_o/(0.6\,\lambda) \quad \text{eq. (43)}$$

$$= \mu_o/\tau_o \quad \text{eq. (46)}$$

i.e., the shear stress approaches a limit at high shear rates as with lubricating oils.

The temperature function in equation (36) is generally given by the Eyring relation for both lubricating oils and polymers:

$$f_2(T) = Ae^{U/kT} \tag{47}$$

or

$$\frac{\mu}{\mu_o} = e^{\beta\left(\frac{1}{T} - \frac{1}{T_o}\right)} \tag{48}$$

Cogswell [97] lists the relative fluidity index

$$RFI = \frac{\mu \text{ at } T°C}{\mu \text{ at } T + 10°C} \tag{49}$$

for a number of polymers, see Table 2:

It is straight forward to show that

$$\beta = \frac{\ell n(RFI)}{\frac{1}{T} - \frac{1}{T + 10°K}} \tag{50}$$

The effect of increased pressure on viscosity is similar to a decrease in temperature i.e., reducing free volume and molecular mobility so leading to an increase in viscosity. The study of the influence of pressure on viscosity has attracted few experimentalists or detailed reviews. This is because the primary interest in polymer properties is extrusion processes where the pressures of several hundred psi are insufficient to influence viscosity. As with lubricating oils

$$\frac{\mu}{\mu_o} = e^{\alpha p + \beta\left(\frac{1}{T} - \frac{1}{T_o}\right)} \tag{51}$$

Since

$$d\mu = \left(\frac{\partial \mu}{\partial p}\right)_{\mu_o} dp + \left(\frac{\partial \mu}{\partial T}\right)_{\mu_o} dT$$

or

$$\left(\frac{dT}{dp}\right)_{\mu_o} = \alpha T_o^2/\beta \tag{52}$$

Cogswell [97] has given a table of the pressure/temperature equivalence at constant viscosity as well as constant entropy to suggest a guide if only the thermodynamic data is available. The table is reproduced below. With Table 3 and equation (52), the pressure coefficient can be found for a number of polymers.

4. ADOPTED MODEL

Both the lubricating oils (under high pressures) and the polymers have similar properties and have similar mathematical descriptions. They show elastic behavior (memory) during short time scales so that equation (29) is the fundamental starting point for a model. A classic text on the viscoelastic properties of melt polymers is written by Ferry [98]. He gives an expression which relates the elastic shear modulus G to the molecular weight distribution of the polymer:

TABLE 2. RELATIVE FLUIDITY INDEX (RFI) FOR AN INCREASE IN TEMPERATURE OF 10°C

Polymer	Test temperature (°C)	RFI*
Branched polyethylene	150	1·35
	200	1·3
	250	1·25
Linear polyethylene	200	1·2
Polypropylene	200	1·2
Polystyrene	200	1·7
Polymethyl methacrylate	200	2·5
	250	1·9
Polycarbonate	250	1·5
Polyethersulphone	350	1·5
Nylon 6:6	275	1·35
Polyethylene terephthalate	275	1·35
Polyacetal	200	1·2
Polyvinylchloride	200	3·0†

* $\text{RFI} = \frac{\text{viscosity at } T\,^{\circ}\text{C}}{\text{viscosity at } (T+10)\,^{\circ}\text{C}}$ at constant stress.

† In the case of polyvinylchloride the 'melt' is known to be slightly crystalline.

TABLE 3. RATIO OF VISCOSITY TO ENTROPY OF VARIOUS POLYMERS

Polymer	$(\Delta T/\Delta P)_\eta$ (°C/Nm^{-2})	$(\delta T/\delta P)_S$ (°C/Nm^{-2})	Ratio η/S
Low-density polyethylene	$5{\cdot}3 \times 10^{-7}$	$1{\cdot}6 \times 10^{-7}$	3·3
High-density polyethylene	4·2	1·5	2·8
Polypropylene	8·6	2·2	4·0
Polystyrene	4·0	1·5	2·7
Poly(methyl methacrylate)	3·3	1·2	2·8
PVC	3·1	1·1	2·8
Nylon	3·2	1·2	2·7
Silicone	6·7	1·9	3·5
Acetal copolymer	5·1	1·4	3·6
Polyphenylene oxide	5·7	—	—
Polycarbonate	3·6	—	—
Polyethersulphone	6·7	—	—
Average value	5·0 SD 1·7	1·4 SD 0·4	3·1 SD 0·5

$$\frac{1}{G} = \frac{0.4\ \bar{M}_W}{\rho RT} \qquad (53)$$

where $\bar{M}_W$ is the weight average molecular weight as opposed to $\bar{M}_N$, the number average, and R is the gas constant. Generally, the modulus is on the order of 10^5 pa (15 psi) for both lubricating oils and polymers

Polymer models must have Newtonian behavior at low rates of shear and limiting shear stress at high rates of shear. Between these two limits a number of empirical models have been reviewed above. Often, there is little to choose between them when selecting the proper experimental constant. Since rotating bands operate in very high shear rate regions where limiting shear stresses exist near the moving surface, it is proposed to use the more direct (and, mathematically, the least complex) low and high shear rate asymptotes. Thus,

$$\frac{du}{dy} = \frac{d}{dt}\left(\frac{\tau}{G}\right) + F(\tau) \qquad (54)$$

where

$$F(\tau) = \frac{\tau}{\mu}\ ; \qquad \tau < \tau_L$$

$$= \frac{\tau}{\tau_L}\frac{du}{dy} \qquad \tau = \tau_L$$

or

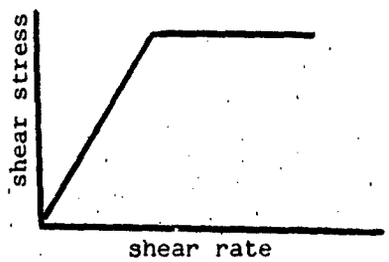

SECTION IV

FRICTION THEORY FOR METAL ROTATING BANDS

1. INTRODUCTION

Evidence of material melt at contact points of rubbing surfaces is well documented by Bowden and Tabor [14]. That full melt occurs over the surface at high sliding speeds is not surprising. Bowden and Freitag [47] found a melt over the contact surface of metals touched by spinning steel balls. Sternlicht and Apkarian [45] gave evidence of melt with the Franklin Institute pin-disk machine. Montgomery [9][10] proposed a full-film melt for projectile rotating bands.

Under large loads full-film melt can take place at low sliding speeds. Tanaka [40] reported a thin layer of melt on polymer pins when rubbed with steel and glass surfaces at speeds to 2.5 m/sec. Recently Clerico [38] found the presence of a solidified melt on rotating polyacetal disks at relative sliding speeds of 0.76 m/sec.

Theoretical papers on melt lubrication are limited. Wilson [42] proposed a hydrodynamic slider bearing model of the slider riding on its own melt. The fluid temperature was assumed to be constant at the melt temperature, and no consideration was given to heat transfer from the melt region. Bicego, et al. [43] modified Wilson's work to include conduction from the surface (ice) to the film. The results were obtained in terms of the track-slider temperature difference, thus avoiding the actual heat conduction problem. There is no a priori reason to assume that non-parallel surfaces (hydrodynamic effect) are necessary to produce load support for melt lubrication. In early experiments using the Franklin Institute pin-disk machine, Sternlicht and Apkarian [45] measured the friction and wear of several metal pins against a high speed steel disk. In an application of Reynolds' equation to melt lubrication, they proposed the thermal wedge as the mechanism to support a normal load between parallel surfaces. Neither the basic equations nor the solution details were offered in the paper.

The author would like to present an overlooked mechanism to provide load support for parallel surfaces undergoing melt lubrication--the mass melt itself per unit area. The mechanism is similar to the load support achieved with porous bearings.

2. ANALYSIS

The following assumptions are now made but verified through the course of the section.

1) The fluid is laminar and incompressible.
2) The pressure is constant across the film and average values of density and viscosity are employed.
3) Film thickness and melt penetration into the solid are small compared to the length and width of the slider.
4) Only one surface is melting. Resolidification occurs after the melt flows from between the surfaces.
5) Quasi steady-state conditions are reached in the film.

The basic equations for thin films are taken from Constantinescu [10].

Momentum

$$\frac{\partial p}{\partial x} = \frac{\partial}{\partial y}\left(\mu \frac{\partial u}{\partial y}\right) \tag{55}$$

$$\frac{\partial p}{\partial z} = \frac{\partial}{\partial y}\left(\mu \frac{\partial w}{\partial y}\right) \tag{56}$$

Since the pressure is independent of y, the above equations may be integrated to give expressions for the velocities u, w between the two surfaces. For a slider moving with velocity U across a fixed plane,

$$u = \frac{1}{2\mu}\frac{\partial p}{\partial x}(y^2 - yh) + \frac{Uy}{h} \tag{57}$$

$$w = \frac{1}{2\mu}\frac{\partial p}{\partial z}(y^2 - yh) \tag{58}$$

where h is the film thickness.

Continuity

$$\frac{\partial(\rho u)}{\partial x} + \frac{\partial(\rho w)}{\partial z} + \frac{\partial(\rho v)}{\partial y} = 0 \tag{59}$$

When the continuity equation is integrated across the film, the resultant equation is called Reynolds' equation:

$$\frac{\partial}{\partial x}\left(\frac{\rho h^3}{\mu}\frac{\partial p}{\partial x}\right) + \frac{\partial}{\partial z}\left(\frac{\rho h^3}{\mu}\frac{\partial p}{\partial z}\right) = 6U\frac{\partial}{\partial x}(\rho h) + 12[\rho v]_o^h \qquad (60)$$

Typically in such derivations the term ρv is replaced by the surface rate of approach, $\rho\partial h/\partial t$, and the film is referred to as a "squeeze film." Previous models of melt lubrication have proposed hydrodynamic action, $h(x)$, or thermal wedge action, $\rho(x)$, to account for film load support. However, it is a mistake to assume that the last term in equation (60) is zero if the surfaces do not approach each other. The term should be interpreted as the rate of mass addition per unit area from the melting surface. Then for parallel surfaces and a fluid with constant density and viscosity equation (60) becomes

$$\nabla^2 p = 12\mu\,\dot{m}/\rho h^3 \qquad (61)$$

where $\dot{m}$ is the constant mass rate of melt per unit area for the slider or fixed surface. A solution, analogous to the squeeze film problem [98], is given by

$$p - p_a = \frac{48\dot{m}\ell^2\mu}{\rho h^3\pi^3}\sum_{n=1,3,5}^{\infty}(-1)^{(n-1)/2}\,n^{-3}\left[\frac{\cosh(n\pi z/\ell)}{\cosh(n\pi\beta/2)} - 1\ \cos(n\pi x/\ell)\right] \qquad (62)$$

where β is the ratio of the long side length to the short side length ℓ. The load support is found by integrating equation (62) over the area A.

$$\sigma = \frac{W}{A} = \frac{\mu\dot{m}\ell^2}{\rho h^3}\left[1 - \frac{192}{\pi^5\beta}\sum_{n=1,3,5}^{\infty} n^{-5}\tanh(n\pi\beta/2)\right] \qquad (63)$$

or

$$\sigma = \mu\dot{m}\ell^2\delta/\rho h^3 \qquad (64)$$

where δ is equal to one for large β.

Energy

The energy equation is

$$\rho c \frac{DT}{Dt} = k\nabla^2 T + \Phi \qquad (65)$$

where Φ is the dissipation function. By dimensional reasoning the film is quasi steady-state if the characteristic time of the process $t_c >> h^2/\alpha$. Furthermore, gradients across the thin film are much greater than gradients in the film plane, and the latter are neglected in thin film lubrication [99]. Thus,

$$k \frac{\partial^2 T}{\partial y^2} + \mu\left[\left(\frac{\partial u}{\partial y}\right)^2 + \left(\frac{\partial w}{\partial y}\right)^2\right] = 0 \qquad (66)$$

The solution is found by substituting equations (57)(58) into equation (66) and integrating twice. However, a simplification can be made. In all pratical cases the viscous heating due to the squeeze velocity, which arises from the pressure gradients, is negligible when compared to the heating due to the sliding velocity. Assuming

$$\frac{h}{2u}\frac{\partial p}{\partial x} /(U/h) = \frac{\sigma h^2}{\mu \ell U \delta} << 1 \qquad (67)$$

then

$$T - T_f = (T_s - T_f)y/h - \frac{\mu U^2}{2kh^2}(y^2 - yh) \qquad (68)$$

where T_s, T_f are the surface temperatures of the slider and fixed surface respectively.

The heat flux per unit area out of the film can be established from the temperature gradient at the surface:

$$q_s = -k[dT/dy]_h$$

$$q_f = +k[dT/dy]_o$$

or

$$q_s = k(T_f - T_s)/h + \mu U^2/2h \qquad (69)$$

$$q_f = -k(T_f - T_s)/h + \mu U^2/2h \qquad (70)$$

At the same time the heat flux into the surfaces depends upon whether or not the surface is melting. Landau [100] has solved the transient heat conduction problem for a melting solid in which the melt is continuously removed. He showed that melting commences at time

$$t_m = \alpha[\rho Ha/q]^{1/2} \tag{71}$$

where α is the diffusivity, H is the latent heat of fusion,

$$a = \pi^{1/2}\, c(T_m - T_o)/2H \tag{72}$$

and T_m is the melt temperature. For rubbing solids,

$$q = f\sigma U \quad \text{(rubbing solids)} \tag{73}$$

where σ is the load per unit area, and f is the friction coefficient. For highly stressed metal surfaces rubbing at moderate speeds, t_m is on the order of 10^{-8} sec. Landau notes that a steady-state solution, i.e., a state characterized by the migration inward at a constant velocity of a fixed temperature distribution in the solid, exists with the heat flux:

$$q_m = \dot{m}[H + c(T_m - T_o)] \quad \text{(melt surface)} \tag{74}$$

The approximate condition at which this steady-state is reached is $t = 10\, t_m$ for $a \geq 1$. With smaller values (of a) the time is longer. At the solid surface the heat flux for transient conduction in a semi-infinite solid is

$$q = \frac{k'(T_{s,f} - T_o)}{(\pi\alpha' t)^{1/2}} \tag{75}$$

Using the average heat flux over the characteristic contact time $t_c = \ell_c/U$ where the characteristic length ℓ_c is L for the fixed surface and x_o (the sliding distance) for the slider,

$$q_{nm} = 2q = \frac{2k'(T_{s,f} - T_o)}{(\pi\alpha'\ell_c/U)^{1/2}} \quad \text{(non-melt surface)} \tag{76}$$

The reader is cautioned that non-melting sliders undergoing extremely large sliding distances should be modeled as a steady-state conduction problem governed by convection heat transfer coefficients at the boundary.

Once it is determined which surface melts, equations (69) and (70) are equated to the proper flux, equations (74) and (76). The resulting two equations can be solved for film thickness h and surface tempera-

ture T_f or T_s, depending upon which one has been replaced by the melt temperature T_m. The results show that the same governing equations apply to a melting slider or a melting fixed plane:

$$(T_{s,f} - T_o) = [(T_m - T_o) + \phi_3]/(1 + b_2 h) \tag{77}$$

$$b_1 b_2 h^5 + b_1 h^4 + b_2[(T_m - T_o) - \phi_3]h - 2\phi_3 = 0 \tag{78}$$

where

$$b_1 = \sigma[(H/c) + (T_m - T_o)]/\alpha\mu\ell^2\delta \tag{79}$$

$$b_2 = 2k'(\pi\alpha'\ell_c/U)^{-1/2}/k \tag{80}$$

$$\phi_3 = \mu U^2/2k \tag{81}$$

The solution to the problem can be simplified if the non-melting surface is conducting or non-conducting. The total heat flux from the film is divided between the melting and the non-melting surfaces:

$$q_s + q_f = q_m + q_{nm} \tag{82}$$

From equations (69) and (70),

$$q_s + q_f = \mu U^2/h \tag{83}$$

Now the heat transfer ratio

$$\frac{q_m}{q_{nm}} = \frac{\rho c h^3[H + c(T_m - T_o)]}{2\mu\ell^2\delta k'(T_m - T_o)} \left(\frac{\pi\alpha'\ell_c}{U}\right)^{1/2} \tag{84}$$

represents two extreme approaches: (i) $q_m/q_{nm} << 1$ where most of the generated heat is conducted into the non-melting surface, and (ii) $q_m/q_{nm} >> 1$ where most of the generated heat goes to melting the opposing surface. Although many conditional factors affect the ratio in equation (57), the author has found that surfaces with high thermal conductivity (metals) tend to give a solution that forms a low ratio although high sliding velocities for all material pairs will do the same. Using the words "conducting surface" and "non-conducting surface" to characterize the approaches, two extreme solutions can be obtained for the film thickness. If $q_m/q_{nm} << 1$, then

$$\mu U^2/h = q_{nm} \tag{85}$$

For most cases equation (77) reduces to

$$(T_{s,f} - T_o) = (T_m - T_o)$$

Thus, the film thickness for a conducting, non-melting surface is

$$h = \frac{\mu U^2(\pi\alpha'\ell_c/U)^{1/2}}{2k'(T_m - T_o)} \tag{86}$$

Similarly, if $q_m/q_{nm} >> 1$, then

$$\mu U^2/h = q_m \tag{87}$$

Thus, the film thickness for a non-conducting, non-melting surface is

$$h = \left\{ \frac{(\mu U\ell)^2\delta}{\rho\sigma[H + c\,(T_m - T_o)]} \right\}^{1/4} \tag{88}$$

Once equation (86) or equation (88) is selected to find the film thickness, equation (84) can be used to verify that the corresponding heat transfer ratio is satisfied. If the ratio is near unity, the fifth order polynomial, equation (78), must be solved for the film thickness.

3. FRICTION FORCE

Again neglecting the contribution of the pressure gradient to the flow field, the force per unit area on the slider is simply

$$\tau = \frac{\mu U}{h} \tag{89}$$

The coefficient of melt friction is

$$f = \frac{\mu U}{h\sigma} \tag{90}$$

The two extreme solutions for the film thickness yield

$$f = \frac{2k'(T_m - T_o)}{\sigma(\pi\alpha'\ell_c U)^{1/2}} \quad \text{(conducting surface)} \tag{91}$$

$$f = \left\{ \frac{\mu^2 U^2 \rho[H + c(T_m - T_o)]}{\ell^2\sigma^3\delta} \right\}^{1/4} \quad \text{(non-conducting surface)} \tag{92}$$

The importance of material thermal properties is evident. Furthermore, low sliding velocities suggest an increasing coefficient of friction with speed, equation (92), whereas high sliding velocities

suggest a decreasing coefficient of friction with speed, equation (91). These effects have been noted in data for the dry sliding of polymers [35][36].

4. WEAR

The material wear is represented by the amount of melt squeezed out from the contact area, $\dot{m}$, and is given by equation (64). Expressed as the volume removed per unit distance travel

$$V(cm^3/cm) = \frac{Wh^3}{\ell^2 \mu U \delta} \qquad (93)$$

5. EXAMPLES

The melt lubrication model is now applied to two examples: (1) a copper rotating band melting on a steel gun barrel; (2) an ice skater. Each example represents conducting surfaces.

Rotating bands have no flow in the circumferential direction while an ice skate is very narrow. In each case β is infinity. The non-melting steel has a characteristic contact length ℓ_c equal to the rotating band width when it is the barrel, but it has a characteristic contact length ℓ_c equal to the skater's stroke when it is the slider. Table 4 lists appropriate variables. Melted copper properties were obtained from Sternlicht and Apkarian [45]. A summary of the two examples is given in Table 5.

The Reynolds' number R is indeed small, and the temperature across the film differs little from the melt temperature. Thus, assumptions (1) and (2) are justified. Density changes sufficient to cause a thermal wedge action is remote. It remains to verify that the pressure gradient contribution to the energy equation (66) is negligible when compared to the Couette contribution. The parameter in equation (67) has a magnitude of approximately 10^{-3} for the two examples above.

Montgomery [10] found indirectly that the friction coefficient of gilding metal (90% Cu; 10% Zn) rotating bands in 155 mm howitzers decays rapidly to f = 0.020 within 12 cm of travel. Using his speed, 9000 cm/sec, at which this value is reached and the band width, 2 6 cm, the calculated value of the friction coefficient is 0.024. Montgomery notes that "the coefficient of friction slowly falls with increased travel beyond this point but this probably was an artifact caused by

neglecting the wear of the rotating bands." Although this explanation is a factor, it is significant that the expression for the friction coefficient, based on equation (91), decays as the square root of the velocity. This phenomenon would be expected as the projectile accelerates down the barrel.

TABLE 4. VARIABLES FOR MELT LUBRICATION EXAMPLES

Parameter	Melted Copper	Melted Ice	Solid Steel
U (cm/sec)	3.0×10^4	100	
σ (N/cm^2)	3.4×10^4	100	
H (N-cm/kg)	$1\ 17 \times 10^6$	1.90×10^7	
$T_m - T_o$ (°C)	1055	2	
α (cm^2/sec)	0.9	1.30×10^{-3}	0.09
c (N-cm/kg-°C)	4.3×10^4	4.3×10^5	
k (N/sec-°C)	354	0.55	33
ρ (kg/cm^3)	8.9×10^{-3}	1×10^{-3}	
μ ($N\text{-}sec/cm^2$)	3.3×10^{-7}	1.7×10^{-7}	
ℓ (cm)	0.7	0.3	
ℓ_c (cm)			0.7 (fixed) 150 (slider)
b_1 (°C/cm^4)	2.6×10^{14}	4.1×10^{14}	
b_2 (cm^{-1})	72	183	
ϕ_3 (°C)	0.42	3.1×10^{-3}	

TABLE 5. SUMMARY OF EXAMPLES

Example	h (cm)	$T_{s,f} - T_m$ (°C)	f	R
rotating band	1.1×10^{-5}	0.4	0.026	90
skater	1.7×10^{-5}	3×10^{-3}	0.011	0.1

(The reverse of this page is blank.)

SECTION V

FRICTION THEORY FOR METAL PIN-ON-DISK DEVICES

1. INTRODUCTION

Friction theories have been based on material mechanical properties and limited to low speeds. However, in most engineering applications frictional heating is significant. It has been known for decades that dry rubbing between bodies produces very high temperatures at the asperities sufficient to melt the material [14]. Early high speed sliding experiments at the Franklin Institute [101] have found molten layers between metal pins rubbed on steel disks, the data subsequently summarized by Montgomery [9]. Recent workers [35][38][39] have reported evidence of melt layers when polymer pins are rubbed on steel and glass disks (or cylinders) where the relative sliding velocities are on the order of one m/s.

Stiffler [12] derived a melt theory to explain friction and wear between sliding surfaces, applying it to projectile rotating bands. The essential features of the theory are the following.

1) Dry rubbing at sufficient loads and speeds will produce enough heat to melt one surface.
2) Once a layer of melt forms a steady-state condition exists in which viscous friction supplies the heat to melt one member of the sliding pair.
3) The load support is governed by classic squeeze film principles, but the melt is continually supplied to maintain a constant film thickness.
4) The melt thickness must exceed the non-melting surface roughness.

The purpose of this paper is to extend the rectangular theory to cylindrical contacts and apply the results to pin-on-disk data. The theory development will parallel Section IV.

2. ANALYSIS

Consider a round pin sliding on a rotating disk in which the disk has a higher melting point than the pin. The following assumptions are employed to describe the melt.

1) The fluid is laminar and incompressible.

2) The pressure is constant across the thickness h, and the density and viscosity are constant throughout the film.

3) The pin is melting with resolidification after squeezing from the contact.

4) The surfaces remain parallel.

5) Film thickness and heat penetration into the solid are small compared to the pin size.

6) Quasi-steady state conditions are reached in the film.

Assumptions (5) and (6) are justified by the theoretical heat transfer work of Landau [100] and summarized in Section IV.

Although the round pin suggests cylindrical coordinates and the sliding velocity boundary condition suggests rectangular coordinates, a difficult two-dimensional problem can be avoided by using the superposition principle [102], i.e., the non-linear inertia terms are neglected in lubrication fluid mechanics. Thus, the pressure and velocity fields for the "Couette effect" due to pin translation can be added to the fields for the radial "squeeze effect."

The Couette effect develops no pressure field or load support. The velocity is simply

$$v_x = Uy/h \tag{94}$$

where x denotes the direction of disk surface velocity U and y denotes the direction perpendicular to the surfaces.

The momentum equation for the squeeze effect is

$$\frac{\partial p}{\partial r} = \mu \frac{\partial^2 v_r}{\partial y^2} \tag{95}$$

Integrating across the melt film for a stationary disk and pin,

$$v_r = \frac{1}{2\mu} \frac{\partial p}{\partial r} (y^2 - yh) \tag{96}$$

The continuity equation is

$$\frac{1}{r} \frac{\partial(\rho r\, v_r)}{\partial r} + \frac{\partial(\rho v_y)}{\partial y} = 0 \tag{97}$$

Substituting equation (96) and integrating across the film gives the reduced Reynolds' equation for parallel surfaces:

$$\frac{1}{r}\frac{d}{dr}\left[r\frac{dp}{dr}\right] = \frac{12\mu}{\rho h^3}\left[\rho v_y\right]_o^h \tag{98}$$

$$p(R) = p_a$$

$$\frac{dp(0)}{dr} = 0$$

The term v_y at the surface is always interpreted as the rate of surface approach $\partial h/\partial t$, i.e., a squeeze film. However, in this case, the term $\rho v_y = \dot{m}$ must be interpreted as the rate of mass addition per unit area from the melting pin.

The solution is given by

$$p - p_a = \frac{3\mu\dot{m}}{\rho h^3}(R^2 - r^2) \tag{99}$$

Integrating over the pin area for the load capacity,

$$W = \frac{3\pi\mu\dot{m}R^4}{2\rho h^3} \tag{100}$$

or

$$\sigma = \frac{3\mu\dot{m}R^2}{2\rho h^3} \tag{101}$$

where σ is the average pressure between the pin and disk.

It is viscous dissipation in the melt layer that supplies the energy to continually generate pin melt. In addition, energy is lost from the film by way of transient heat conduction into the non-melting disk surface. The film thickness (degree of melt) depends on the distribution of heat between the pin and disk. Since the characteristic time of the film heating (h^2/α) is much smaller than the pin contact time, the film heating is quasi-static. Furthermore, only gradients perpendicular to the surfaces are important (assumption 5). Thus, the energy equation for the melt layer reduces to

$$k\frac{d^2T}{dy^2} + \mu\left[\left(\frac{dv_r}{dy}\right)^2 + \left(\frac{dv_x}{dy}\right)^2\right] = 0 \tag{102}$$

Now in all practical cases the pin translational velocity v_x is much greater than the squeeze velocity v_r, and viscous heating from the latter is neglected. Assuming

$$\frac{dv_r/dy}{dv_x/dy} = \frac{dh^2\sigma}{\pi\mu RU} << 1$$

the solution to the energy equation is

$$T - T_m = (T_d - T_m)(y/h) - \frac{\mu U^2}{2kh^2}(y^2 - yh) \qquad (103)$$

where T_d and T_m are the surface temperatures of the disk and melting pin respectively.

The heat transfer per unit area <u>out</u> of the film is given by the temperature gradient at the surface:

$$q_p(pin) = +k[dT/dy]_o$$

$$q_d(disk) = -k[dT/dy]_h$$

or

$$q_p = -k(T_m - T_d)/h + \mu U^2/2h \qquad (104)$$

$$q_d = +k(T_m - T_d)/h + \mu U^2/2h \qquad (105)$$

What is the heat transfer in equations (104) and (105)? For the melting pin the work of Landau [100] is important. He found that the problem of a heat flux imposed on a surface where the melt is continually removed will reach a steady state solution within a time scale much less than the contact time. The state is characterized by a steady inward migration of a fixed temperature distribution within the solid, and the heat transfer is given by

$$q_p = \dot{m}[H + c(T_m - T_o)] \qquad (106)$$

At the disk surface the heat transfer for transient conduction into a semi-infinite solid is

$$q = \frac{k'(T_d - T_o)}{(\pi\alpha' t)^{1/2}} \qquad (107)$$

where the prime represents disk properties. For a pin with characteristic length ℓ_c sliding on a disk at relative velocity U, the characteristic contact time $t_c = \ell_c/U$. Using the average heat flux for the contact time,

$$q_d = 2q = \frac{2k'(T_d - T_o)}{(\pi\alpha'\ell_c/U)^{1/2}} \tag{108}$$

Since contact length varies across the pin an average contact length is defined:

$$\ell_c = \frac{2R}{\pi/2}\int_0^{\pi/2} \cos\theta d\theta = \frac{4}{\pi}R \tag{109}$$

Equations (104) and (105) may be solved now for the two unknowns: disk surface temperature T_d and film thickness h;

$$(T_d - T_o) = [(T_m - T_o) + \phi_3]/(1 + \phi_2 h) \tag{110}$$

$$\phi_1\phi_2 h^5 + \phi_1 h^4 + \phi_2[(T_m - T_o) - \phi_3]h - 2\phi_3 = 0 \tag{111}$$

where

$$\phi_1 = 2\sigma[(H/c) + (T_m - T_o)]/3\alpha\mu R^2 \tag{112}$$

$$\phi_2 = 2k'(\pi\alpha'\ell_c/U)^{-1/2}/k \tag{113}$$

$$\phi_3 = \mu U^2/2k \tag{114}$$

For all practical cases,

$$(T_d - T_o) = (T_m - T_o) \tag{115}$$

Equation (111) for the film thickness has a simple solution for two extreme conditions: (1) $q_p/q_d \ll 1$ where most of the generated heat is conducted into the disk, called a conducting disk surface; (2) $q_p/q_d \gg 1$ where most of the generated heat goes to pin melt, called a non-conducting disk surface. This ratio is

$$\frac{q_p}{q_d} = \frac{\rho\sigma h^3[H + c(T_m - T_o)]}{3\mu R^2 k'(T_m - T_o)}\left(\frac{4\alpha' R}{U}\right)^{1/2} \tag{116}$$

While there are many parameters, the film thickness is the predominant term. These film thicknesses are very small and the ratio is much less than one for all pairs examined by the author. For example, low melting nylon pins sliding on a glass disk at one m/s gives a ratio of 10^{-2}.

From equations (104) and (105)

$$q_p + q_d = \mu U^2/h \tag{117}$$

For a conducting disk, $q_p/q_d << 1$, the film thickness is

$$h = \frac{\mu U^2(\alpha' R/U)^{1/2}}{k'(T_m - T_o)} \tag{118}$$

For a non-conducting disk, $q_p/q_d >> 1$, the film thickness is

$$h = \left\{\frac{3(\mu UR)^2}{2\rho\sigma[H + c(T_m - T_o)]}\right\}^{1/4} \tag{119}$$

3. FRICTION FORCE

The friction force per unit area is

$$\tau = \frac{\mu U}{h} \tag{120}$$

The coefficient of melt friction is

$$f = \frac{\mu U}{h\sigma} \tag{121}$$

The two extreme conditions for the film thickness yield

$$f = \frac{k'(T_m - T_o)}{\sigma(\alpha' RU)^{1/2}} \quad \text{(conducting disk)} \tag{122}$$

$$f = \left\{\frac{2\mu^2 U^2 \rho(H + c(T_m - T_o)}{3R^2\sigma^3}\right\}^{1/4} \quad \text{(non-conducting disk)} \tag{123}$$

4. WEAR

The material wear is represented by the amount of melt $\dot{m}$ squeezed from the contact area and is given by equation (101). Expressed as the volume removed per unit distance of travel:

$$V(cm^3/cm) = \frac{2\pi\sigma h^3}{3\mu U} \tag{124}$$

5. RESULTS

Perhaps the most comprehensive experimental study of metal friction and wear at high sliding speeds was done at the Franklin Institute from 1946 to 1956. A pin-on-disk device was used to slide metal pins aganst a spinning steel disk at speeds up to 548 m/s. The pins were primarily copper and gilding metal (90 CU; 10 ZN) although several runs exist for aluminum, zinc, and nylon. A radial pin displacement on the disk assured that all data were single pass. This fact is important for comparisons between theory and experiment.

A calculation of the heat transfer ratio showed that the disk is conducting for all test parameters. Therefore, a normalized coefficient of friction, based on equation (29), is defined:

$$\bar{f} = \frac{f_o \sigma (\alpha' RU)^{1/2}}{k'(T_m - T_o)} \qquad (125)$$

where f_o is the measured coefficient of friction. The data plotted against f should reduce to one. Thermal properties [103] of the gun steel disk can vary significantly with temperature:

T(°C)	27	250	400	600	1250
$k'\left(\frac{N}{sec°C}\right) = 1.73 \times \frac{Btu}{hr\ ft\ °F}$	43	40	36	33	32
$\alpha'(cm^2/sec)$	0.122	0.092	0.073	0.058	0.063

Since the heat flux is defined at the disk surface, the thermal conductivity in equation (125) should be the value at the pin melting temperature. However, the disk diffusivity covers the range from T_m to T_o, and an average diffusivity (not the diffusivity at the average temperature) is used. It is assumed that the disk bulk temperature T_o is 27°C.

A plot of normalized coefficient of friction versus pin pressure is shown in Figure 27 for a wide range of sliding velocities. The majority of the data represents copper pins with a diameter of 0.2031 cm. The available data for aluminum, zinc, and nylon was limited to 274 m/sec with a pin diameter of 0.3556 cm. There is a rather remarkable fit for copper at the higher pin pressures and a tight

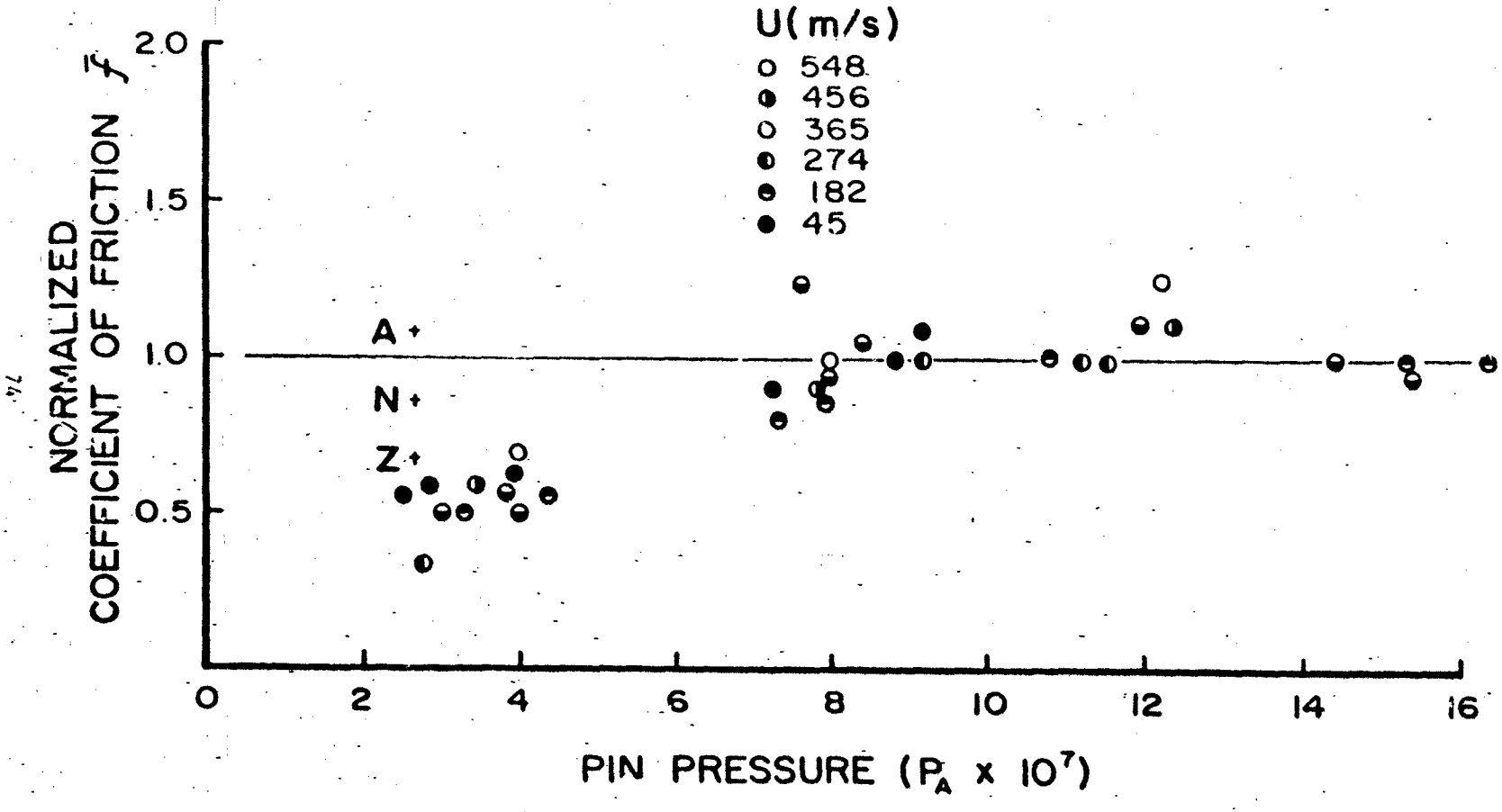

Figure 27. Experimental over Theoretical Coefficient of Friction as a Function of Sliding Speed and Load per Unit Area

correlation with sliding velocity at all pin pressures. The measured coefficient of friction at lower pin pressures is smaller than the coefficient predicted by theory. The reason is the disk roughness.

Shugarts and Rippel [101] reported that the Franklin Institute test disk had an rms roughness of 5 - 13μcm (2 - 5μin) in the direction of travel. The copper film thickness was calculated from equation (118), using a melt viscosity of 3 3 x 10^{-7} N-sec/cm^2; h = 8μcm. Under very high pin pressures the disk asperities are greatly deformed and the surface roughness is reduced. At lower pin pressures the copper film thickness and the disk asperities are comparable and the film is no longer uniform over the pin surface. Thus, the pressure is larger than the calculated value using the pin area, and the coefficient of friction will be smaller. In effect the normalized coefficient of friction for copper at low pressures is less than the theoretical value because the melt layer is incomplete, and the pressure σ is based on the pin area, not on the actual contact area. The lower melting point nyion and aluminum produce thicker melt films and give satisfactory results at the lower pin pressures. However, the data for zinc is inconsistent with these findings.

The wear rates of the copper pins were tabulated also for the Franklin Institute tests [9]. These experimental wear rates were approximately 10^{-6} cm^3/cm. When the theoretical wear rate from equation (31) was calculated, it was found to be approximately 10^{-8} cm^3/cm. Wear rates are difficult to compare because of the sensitivity of the wear rate to the melt viscosity. It is certain that the viscosity is much higher than the number used here because of the very high pin pressures. Also, the high shear rates are a factor. No information appears to be available on how these two parameters affect the viscosity of metals.

Contact Area

The friction coefficient can be lowered by increasing the contact stress either by (1) decreasing the pin area, or (2) increasing the number of contacts, i.e., a surface with a roughness exceeding the melt thickness. Assume N contacts of radius a. Then equation (122) becomes

$$f = \frac{\bar{N}\pi a^{3/2} k'(T_m - T_o)}{W(\alpha' U)^{1/2}} \qquad (126)$$

where W is the known load. The coefficient of friction decreases with the number and size of the contacts until the flow pressure σ_f of the softer surface is reached. The latter state is achieved for most rough surfaces under light loads and slow sliding speeds where the melt thickness is much less than the roughness height. Gupta and Cook [104] have investigated several pairs of mating rough surfaces and found that the number of contacts is nearly proportional to the load while the size of the contact is nearly independent of the load, assuming round asperities of equal size. They found that the ratio of flow pressure to hardness falls between 0.50 - 0.55. Replacing the contact stress with the flow pressure in equation (122),

$$f = \frac{k'(T_m - T_o)}{\sigma_f(\alpha' a U)^{1/2}} \qquad (127)$$

where

$$a = 4R \times 10^{-3}/\sqrt{\zeta} \qquad (128)$$

The topographic index ζ introduced by Gupta and Cook characterizes the roughness:

$$\zeta = \frac{E'}{\beta H_v \sqrt{2N}} \qquad (129)$$

where β is the asperity radius of curvature and N is the number of peaks prior to loading. Thus, the coefficient of friction is a minimum when the contact stress approaches the pin flow pressure, and the size of the individual contact spots is as large as possible while maintaining the high contact pressure. In theory frictional behavior can be improved by dimpling the non-melting surface.

Tanaka and Uchiyama [39] studied the effects of sliding speed on the friction and wear of crystalline polymers. A pin-on-disk device was used for speeds over the range: 10 - 300 cm/s. Overwhelming evidence was presented to support a melt phenomena. Melt depth of polymer pins on a glass disk was on the order of 10^{-2} cm while the depth with a steel disk was only several microns. The heat ratio in equation (23) was much less than one for both glass and steel disks.

Thus, the theoretical coefficient of friction is given by equation (122). Table 6 lists the polymers and compares the theoretical and experimental coefficients of friction for a glass disk. Glass properties [105] are $k' = 1.17$ N/sec-°C and $\alpha' = 0.006$ cm^2/sec.

It is observed that the theoretical coefficient of friction exceeds the experimental values by a factor of three. The measured coefficients are lower than predicted because all tests were multiple pass. Tanaka and Uchiyama reported polymer melt transfer to the disk where polyacetal was the worse offender. They obtained a photograph of the contact surface through the glass disk. There existed a number of narrow striations parallel to the rubbing direction on the frictional surface. These bands were identified as non-contact areas

TABLE 6. FRICTION COEFFICIENTS AND WEAR RATES FOR SEVERAL POLYMERS AGAINST GLASS. (Experimental data from Tanaka and Uchiyama [39].)

Polymer	M.C. (°C)	f (exp.)	f (th.)	$\bar{f}$	V (exp.)	V (th.) cm/cm
Low Density Polyethylene*	115	0.9	2.3	0 39	4×10^{-6}	--
High Density Polyethylene**	135	0.7	2.1	0.33	4×10^{-8}	5×10^{-5}
Polypropylene*	167	1.3	3.5	0.37	1×10^{-7}	3×10^{-5}
Nylon**	250	1.3	4 3	0 30	1×10^{-6}	1×10^{-4}
Polyacetal**	175	0.6	2.9	0.21	3×10^{-7}	2×10^{-5}

* 120 cm/s
** 250 cm/s

due to polymer lumps and film which had adhered to the disk. Therefore, full contact does not occur, and the actual contact pressure is much higher than the pressure calculated from the pin size. The author visually estimates the contact area as less than one half of the pin cross-sectional area. The unknown disk bulk temperature could be important, especially for multiple pass tests.

Theoretical coefficients of friction for the steel disk are approximately 15 - 30. These unusually high values are a sign that (1) very thin films are disrupted by the surface roughness, and high local

pressures exist in the film or (2) low speeds and loads do not supply sufficient energy to bring the contact into the thermal melt regime. Consider again equation (122). If both sides are multiplied by the sliding velocity and rearranged,

$$f\sigma U = q_d \tag{130}$$

i.e., the frictional work input per unit contact area is equal to the transient heat flux to the disk surface. The contact stress must be determined accurately, and the contact must reach melt temperature before equation (112) is valid.

Table 6 compares the theoretical wear rate for several polymers with the experimental values from Tanaka and Uchiyama. Equation (124) has been adjusted for the higher contact pressures and expressed as a change of pin length per unit length of travel. The measured wear rates are smaller than theory by a factor of 100. Polymer viscosities were determined by measuring the solidified melt depth on the pins and by using an expression identical to equation (121). The calculated viscosity agreed with viscometry within shear rate limits. One possible explanation for the difference is the measurement method. A linear differential transformer was used to measure the change in the pin length. There was no discussion of any adjustment made for the transferred polymer lumps on the glass disk.

6. SUMMARY

The proposed melt theory represents a new approach to friction in the thermal regime. A tentative evaluation of the theory can be made based on the limited studies. The theory predicts the coefficient of friction for metal pairs sliding at high loads and speeds under single pass conditions. At typical engineering loads, surfaces with high thermal conductivity, such as metals, produce very thin melts, on the order of the surface roughness. Then the size and pressure of the contact is uncertain and the measured coefficients of friction always are less than the calculated values. A comparison of experimental wear rates with a melt theory of wear was inconclusive. Data on the viscosity of metal melts at high contact pressures and/or rates of

shear are generally not available. In the case of multiple pass contact the effect of transfer debris on idealized flow passages is difficult to assess.

In the case of polymer pin friction and wear a comparison of theory with one particular experiment [39] was inconclusive. Multiple passes lead to the presence of transfer (wear) debris which altered the apparent contact pressure, a necessary parameter in the theory. However, this problem should not occur for the single pass polymer rotating bands. More important, the non-linear behavior of polymer melts calls into question an application of Newtonian flow for these materials. The subject of non-Newtonian friction theory will now be addressed.

(The reverse of this page is blank.)

SECTION VI

FRICTION THEORY FOR PLASTIC ROTATING BANDS

In the previous two sections melt friction theory was derived for Newtonian fluids (in particular metal melts) and applied to copper rotating bands and metal pins. Good agreement between theory and experiment was achieved to confirm the basic approach to the problem. In this section melt friction theory will be derived for polymer melts which display the non-Newtonian fluid behavior discussed in Section III. The fluid is characterized by viscosity, elastic shear modulus, and limiting shear stress, all of which can vary with pressure and temperature.

Although plastic rotating bands are circular the melt films are so thin that a Cartesian coordinate system can be used to analyze the problem. Imagine the thin film cut and spread out in the z-direction with the x-direction of motion as the length. Since the fluid can not flow in the z-direction (the circular band is continuous), the analysis is one-dimensional in the plane of the contact. The rotating band is referred to as the "moving surface" while the barrel is referred to as the fixed surface.

1. MOMENTUM

The analysis is begun with the usual five assumptions at the beginning of Section IV which are characteristic of thin film fluid mechanics in lubrication theory. Since it is no longer possible to start with derived forms of Reynolds' equation for pressure distribution such as equation (60), it is necessary to follow those derivations for the non-Newtonian lubricant.

Neglecting fluid inertia and body forces, the general momentum equations are [46]

$$\frac{\partial p}{\partial x} = \frac{\partial \tau_{xy}}{\partial y} + \frac{\partial \tau_{xz}}{\partial z} \tag{131}$$

$$\frac{\partial p}{\partial y} = \frac{\partial \tau_{xy}}{\partial x} + \frac{\partial \tau_{yz}}{\partial z} \tag{132}$$

$$\frac{\partial p}{\partial z} = \frac{\partial \tau_{xz}}{\partial x} + \frac{\partial \tau_{yz}}{\partial y} \qquad (133)$$

Since the film is thin in the y-direction, $\partial p/\partial y = 0$. Also, the film plane is one-dimensional in the x-direction or $\partial p/\partial z = 0$. In addition, there are no shear stresses in the z-direction. Thus, the above reduces to ($\tau_{xy} = \tau$)

$$\frac{\partial p}{\partial x} = \frac{\partial \tau}{\partial y} \qquad (134)$$

$$0 = \frac{\partial \tau}{\partial x} \qquad (135)$$

With the exception of Conry [106] equation (135) is usually neglected; the consequences are major as discussed below.

Integrating with respect to y and assigning τ_1 as the shear stress at the fixed surface,

$$\tau = y \frac{dp}{dx} + \tau_1 \qquad (136)$$

Now the large contact pressures and large relative sliding at the contacts will assure that the limiting shear stress τ_L will occur at the sliding surface boundary:

$$\tau_1 = \tau_L - h \frac{dp}{dx} \qquad (137)$$

The lubricant shear behavior is described above by the non-linear Maxwell model:

$$\frac{du}{dy} = \frac{U}{G} \frac{d\tau}{dx} + \frac{\tau}{\mu} \qquad \tau \leq \tau_L \qquad (138)$$

From equation (135) it would appear that the elastic term is inoperative. However, let us examine the elastic term more closely. If a small shear strain ζ is considered to be made up of a viscous component ζ_v and an elastic component ζ_e, we have

$$\zeta = \zeta_v + \zeta_e$$

Then from Newton's law of viscosity and Hooke's law of elasticity, the rate of strain is

$$\frac{d\zeta}{dt} = \frac{du}{dy} = \frac{d\zeta_v}{dt} + \frac{d\zeta_e}{dt} \tag{139}$$

or

$$\frac{du}{dy} = \frac{\tau}{\mu} + \frac{d}{dt}(\tau/G) \tag{140}$$

But under steady state conditions

$$\frac{d}{dt} = U\frac{\partial}{\partial x} \tag{141}$$

and

$$\frac{d}{dt}(\tau/G) = U\left[\frac{1}{G}\frac{\partial\tau}{\partial x} - \frac{\tau}{G^2}\frac{\partial G}{\partial x}\right] \tag{142}$$

Since the shear modulus is a function of pressure:

$$G = G_o e^{\kappa p} \tag{143}$$

or

$$\frac{du}{dy} = \frac{\tau}{\mu} - \frac{U\kappa\tau}{G}\frac{\partial p}{\partial x} \tag{145}$$

Substituting equation (136)

$$\frac{du}{dy} = \left[\frac{1}{\mu} - \frac{U\kappa}{G}\frac{dp}{dx}\right]\left[(y-h)\frac{dp}{dx} + \tau_L\right]$$

Integrating with respect to y,

$$u = \left[\frac{1}{\mu} - \frac{U\kappa}{G}\frac{dp}{dx}\right]\left[\left(\frac{y^2}{2} - yh\right)\frac{dp}{dx} + \tau_L y\right] + C \tag{146}$$

The velocity of the fluid is zero at the fixed surface (y = 0); thus, the integration constant is zero. But the boundary condition occurring at the moving surface is the limiting shear stress. The velocity obtained from equation (146) can not agree with the surface velocity; thus, the fluid slips at the moving boundary.

At this point Newtonian lubrication theory substitutes the expressions for velocities, obtained from the momentum equations, into the continuity equation to arrive at Reynolds equation for the film

pressure distribution. Employing the integral form of the continuity for one-dimensional flow with $\dot{m}$ as the mass rate of melt per unit area:

$$\frac{\partial}{\partial x}\int_0^h \rho u dy = \dot{m} \tag{147}$$

and equation (146),

$$\frac{d}{dx}\left[\left(\frac{1}{\mu} - \frac{U\kappa}{G}\frac{dp}{dx}\right)\left(\frac{h^3}{3}\frac{dp}{dx} - \tau_L\frac{h^2}{2}\right)\right] = -\dot{m}/\rho \tag{148}$$

Define dimensionless variables:

$$\bar{p} = pBL/W$$

$$\bar{x} = x/L$$

where B is the rotating band circumference, L is the rotating band length, and W is the load. After employing average values (defined at the average stress) for viscosity μ, shear modulus G, and limiting shear stress τ_L,

$$\frac{d}{d\bar{x}}\left[\left(1 - B_1\frac{d\bar{p}}{d\bar{x}}\right)\left(B_2\frac{d\bar{p}}{d\bar{x}} - 1\right)\right] = -B_o \tag{149}$$

where

$$B_o = 2L\dot{m}\mu/\rho\tau_L h^2$$

$$B_1 = U\kappa\mu W/GBL^2$$

$$B_2 = 2hW/3\tau_L BL^2$$

Boundary conditions for equation (149) are the following:

$$\bar{p}(0) = 0$$

$$\bar{p}(1) = 0$$

A propellant gas pressure exists on the front side of the band, but the pressure is symmetrical and will not contribute to the load support.

Integrate the above equation once to arrive at

$$\left(1 - B_1\frac{d\bar{p}}{d\bar{x}}\right)\left(B_2\frac{d\bar{p}}{d\bar{x}} - 1\right) = -B_o\bar{x} + C_1 \tag{150}$$

The pressure gradient can be found by using the quadratic formula. A second integration gives the pressure distribution. However, the first integration constant is embedded within a radical which makes it impossible to apply boundary conditions and obtain a complete analytical solution. Numnerical methods must be employed. On the otherhand a simplification can be carried out which should be valid for all the physical cases which will occur in practice. Rearranging equation (150):

$$-\left(\frac{d\bar{p}}{d\bar{x}}\right)^2 + \left(\frac{1}{B_1} + \frac{1}{B_2}\right)\frac{d\bar{p}}{d\bar{x}} = -\frac{B_o}{B_1 B_2}x + C_2 \qquad (151)$$

The pressure gradient has been normalized so that its magnitude is on the order of one; thus, the constant parameters dictate the order of the two terms on the left. If <u>either</u> $B_1 \ll 1$ <u>or</u> $B_2 \ll 1$, <u>both</u> of which are probable for melt friction cases, the first term can be neglected and

$$\frac{d\bar{p}}{d\bar{x}} = -\frac{B_o}{(B_1+B_2)}x + C_3 \qquad (152)$$

Integrating

$$\bar{p} = -\frac{B_o}{(B_1+B_2)}\frac{\bar{x}^2}{2} + C_3\bar{x} + C_4 \qquad (153)$$

Applying boundary conditions,

$$\bar{p} = -\frac{B_0}{2(B_1+B_2)}[\bar{x}^2 - \bar{x}] \qquad (154)$$

Now the rotating band must carry load W. Therefore,

$$\int_0^1 \bar{p}\, d\bar{x} = 1 \qquad (155)$$

Completing equation (155),

$$B_1 + B_2 = B_o/12 \qquad (156)$$

The above equation relates the load to the mass rate of melt (and film thickness). The energy equation to follow will give a relationship between the mass rate of melt and film thickness. Together, the film thickness can be found.

2. ENERGY

The energy equation for an element of fluid is a balance between heat conducted into the element, the heat generated through viscous forces, and the rate of change of stored energy:

$$\rho c \frac{DT}{Dt} = k \frac{\partial^2 T}{\partial x^2} + \frac{\partial^2 T}{\partial y^2} + \tau F(\tau) \qquad (157)$$

where the latter term is the viscous dissipation for non-Newtonian fluids [87]. By dimensional reasoning the sliding process is quasi steady-state if the characteristic time of contact is much greater than h^2 ÷ diffusivity. Using the assumption [34] that conduction is much greater across the film than in the direction of motion x,

$$\rho c u \frac{\partial T}{\partial x} = k \frac{\partial^2 T}{\partial y^2} + \tau F(\tau) \qquad (158)$$

For the non-linear Maxwell model of the fluid the term $F(\tau)$ represents the viscous strain rate. Since a model has been adopted that displays a Newtonian viscous strain rate up to the point of slip at the moving surfce where the shear stress is limited to τ_L,

$$F(\tau) = \tau/\mu \qquad (159)$$

In addition, the shear stress and fluid velocity expressions have been derived previously:

$$\tau = (y - h) \frac{dp}{dx} + \tau_L \qquad (160)$$

$$\frac{du}{dy} = \frac{\tau}{\mu} - \frac{U\kappa\tau}{G} \frac{dp}{dx} \qquad (161)$$

Introducing dimensionless numbers

$$\bar{x} = x/L$$

$$\bar{y} = y/h$$

$$\bar{p} = pBL/W$$

$$\bar{\tau} = \tau/\tau_L$$

the above equations are written as

$$P'_e \, \bar{u} \frac{\partial \bar{T}}{\partial \bar{x}} = \frac{\partial^2 \bar{T}}{\partial \bar{y}^2} + \bar{\tau}^2 \frac{\tau_L^2 h^2}{\mu k} \tag{162}$$

$$\bar{\tau} = \frac{3}{2} B_1 (\bar{y} - 1) \frac{d\bar{p}}{d\bar{x}} + 1 \tag{163}$$

$$\frac{d\bar{u}}{d\bar{y}} = \frac{h\tau_L}{\mu U} \left(1 - B_1 \frac{d\bar{p}}{d\bar{x}}\right) \bar{\tau} \tag{164}$$

where

$$P'_e \text{ (reduced Peclet No.)} = \frac{h}{b} \frac{Uh\rho c}{k}$$

The general order of magnitude of the terms in B_1 indicate that it will be much less than one while the very thin melt thicknesses compared to the rotating band size also indicate that the reduced Peclet number and B_2 are much less than one. Then

$$\bar{\tau} \cong 1 \tag{165}$$

$$\frac{d\bar{u}}{d\bar{y}} \cong \frac{h\tau_L}{\mu U} \tag{166}$$

$$0 = \frac{d^2 T}{d\bar{y}^2} + \frac{\tau_L^2 h^2}{\mu k} \tag{167}$$

A small Peclet number not only reduces the partial differential equation to an ordinary differential equation but also uncouples the velocity functional from the energy equation.

Let T_f be the film temperature at fixed surface (barrel) and T_s be the film temperature at the sliding surface (band). Film temperatures are not expected to vary much across the film; thus, parameters are constant with respect to y. Integrating equation (167) and applying boundary conditions (in the form of surface temperatures),

$$T - T_f = (T_s - T_f)\bar{y} - \frac{\tau_L^2 h^2}{2\mu k} (\bar{y}^2 - \bar{y}) \tag{168}$$

Heat transfer per unit area out of the film is expressed in terms of the film temperature gradient at the surface:

$$q_s(x) = -k(dT/dy)_h \tag{169}$$

$$q_f(x) = +k(dT/dy)_o \tag{170}$$

or

$$q_s = -\frac{k}{h}\left[(T_s - T_f) - \tau_L{}^2h^2/2\mu k\right] \tag{171}$$

$$q_f = +\frac{k}{h}\left[(T_s - T_f) + \tau_L{}^2h^2/2\mu k\right] \tag{172}$$

The boundary conditions are completed once the heat flux to the surfaces is known. Heat is transferred by conduction into the solids in amounts q_{NM} at the barrel and q_M at the melting band. When slip occurs at the moving surface, the energy input is $\tau_L U$ while the film receives only $\tau_L U_1$ where U_1 is the surface velocity of the fluid. The difference represents a heat source due to slip. Thus,

$$q_s + \tau_L(U - U_1) = q_M \tag{173}$$

and

$$q_f = q_{NM} \tag{174}$$

Slip velocities can be found by integrating equation (167):

$$U_1 = U\int_0^1 \frac{d\bar{u}}{d\bar{y}}\, d\bar{y} \tag{175}$$

or

$$U_1 = \frac{h\tau_L}{\mu} \tag{175}$$

From Section IV,

$$q_m = \dot{m}[H + c(T_m - T_o)] \tag{177}$$

$$q_{nm} = \frac{2k'(T_f - T_o)}{(\pi\alpha' L/U)^{1/2}} \tag{178}$$

Since $T_s = T_m$ (melting slider) equations (173) and (174) can be solved for the film thickness and barrel surface temperature T_f. Making the proper substitutions into equations (173) and (174) and using equation (156) to define the melt rate m,

$$-(T_m - T_f) - A_0h^2 + A_4h = A_1h^3 + A_2h^4 \tag{179}$$

$$(T_m - T_f) + A_o h^2 = A_3 h(T_f - T_o) \tag{180}$$

where

$$A_o = \tau_L^2/(2\mu k)$$

$$A_1 = 6[H + c(T_m - T_o)]\,\frac{U\kappa W\rho\tau_L}{GBL^3k}$$

$$A_2 = 4[H + c(T_m - T_o)]\,\frac{\rho W}{\mu BL^3k}$$

$$A_3 = \frac{2k'}{k(\pi\alpha' L/U)^{1/2}}$$

$$A_4 = \frac{\tau_L U}{k}$$

Solving for T_f and h,

$$(T_f - T_o) = [(T_m - T_o) + A_o h^2]/(1 + A_3 h) \tag{181}$$

$$A_2A_3h^4 + (A_1A_3 + A_2)h^3 + (A_1 + A_oA_3)h^2 - A_3A_4h + A_3(T_m - T_o) - A_4 = 0 \tag{182}$$

The solution to the problem can be simplified if the surfaces are conducting or non-conducting as defined in Section IV. The ratio of heat transfer to the surfaces is

$$\frac{q_m}{q_{nm}} = \frac{h^2(A_1 + A_2h)}{A_3(T_f - T_o)} \tag{183}$$

If the ratio $q_m/q_{nm} \ll 1$, most of the generated heat given by $\tau_L U$ goes to conduction into the non-melting surface (said to be a conducting barrel surface). Then

$$q_{nm} = U\tau_L \tag{184}$$

Setting $A_1 = A_2 = 0$,

$$A_oA_3h^2 - A_3A_4h + A_3(T_m - T_o) - A_4 = 0 \tag{185}$$

and the quadratic can be solved directly.

If the ratio $q_m/q_{nm} \gg 1$, most of the generated heat goes to melting the rotating band (said to be a non-conducting barrel surface). Then

$$q_m = U\tau_L \tag{186}$$

Substituting from equation (177),

$$A_2h^3 + A_1h^2 = U\tau_L/k \qquad (187)$$

3. FRICTION FORCE

The friction force on the rotating band is the surface shear stress multiplied by the contact area. For the non-Newtonian polymers the shear stress is simply the limiting shear stress τ_L. Then the coefficient of friction is

$$f = \frac{\tau_L BL}{W} \qquad (188)$$

The coefficient of friction decreases for increasing contact pressure as with the metal rotating bands; however, the limiting shear stress is both pressure and temperature sensitive. No distinction is made between the "conducting" and "non-conducting" barrels.

4. WEAR

The material wear is given by the amount of melt squeezed from the contact area, $\dot{m}$, and is given by equation (156). Expressed as the volume removed per unit distance travel:

$$V = \frac{\dot{m}BL}{\rho U} \qquad (189)$$

SECTION VII

EXAMPLE FOR POLYMER BAND

1. ROTATING BAND (30 MM PROJECTILE)

   Material: Polyethersulphone

   Length: $L = 0.5$ in

   Circumference: $B = 37$ in.

   Speed: 10^4 in/sec

2. BARREL PROPERTIES

   $k' = 4.6 \times 10^{-4}$ Btu/sec-in-°F

   $\alpha' = 0.023$ in^2/sec

   Length: 60 in

3. BAND PROPERTIES

   $\rho = 0.035$ lbm/in^3

   $c = 0.5$ Btu/lbm-°F

   $H = 54$ Btu/lbm

   $T_m - T_o = 470$°F

   $k = 9.03 \times 10^{-6}$ Btu/sec-in-°F

   $G = 15$ lbf/in^2 (?)

   $\kappa = 1 \times 10^{-5}$ in^2/lbf (?)

   β (equation 50) = 16,000 1/°K

   α (equation 52) = 0.276×10^{-7} m^2/N (1.9×10^{-4} in^2/lbf)

   μ_o (estimated from similar polymers in reference 39) = 10^{-2} lbf-sec/in^2

   μ (equation 51) = 0.45 lbf-sec/in^2

4. FRICTION

   The coefficient of friction is defined as

   $$f = \tau_L 3L/W$$

However, data on the limiting shear stress of polymers is difficult to find (if it exists). High pressure effects complicate the task. Based upon the author's work [8], it was found that the coefficient of

friction for polyethersulphone rotating bands under conditions similar to actual firings was f = 0.016 at a stress of W/BL = 20,300 lbf/in^2. Thus,

$$\tau_L = 325 \text{ lbf/in}^2$$

5. CONSTANTS

$A_o = 1.4 \times 10^6$ °F/in^2

$A_1 = 5.6 \times 10^{11}$ °F/in^2

$A_2 = 1.0 \times 10^{11}$ °F/in^4

$A_3 = 5.3 \times 10^4$ 1/in

$A_4 = 3.8 \times 10^7$ °F/in

6. MELT THICKNESS

h (equation 186) = 3.8×10^{-6} in

$q_m/q_{NM} = 2.7 \times 10^{-7}$ (i.e., conduct ng surface assumption justified)

$$\dot{m} = \frac{kh^2(A_1 + A_2h)}{H + c\,(T_m - T_o)} = 1.14 \times 10^{-9} \text{ in}^3/\text{in}$$

or 3.7×10^{-8} in layer removed when sliding 5 feet.

SECTION VIII

CONCLUSIONS

Presently accepted sliding friction theories are based upon the concept that microcontacts under high loads instantaneously "weld", and friction is the force to shear these junctions. The subject of sliding velocity does not enter the model, and only a few studies show velocity effects on friction data. The coefficient of friction between sliding pairs is simply given as the shear stress of the "welded" junctions divided by the flow pressure of the softer surface. This number agrees with friction data only qualitatively (surface contamination, oxidation, etc.). However, high sliding speeds produces sufficient surface heat to melt the one surface and form (in 10^{-8} seconds) a melted fluid layer between the surfaces. Fluid mechanics enables one to obtain more accurate expressions for sliding friction and also expressions which are related to sliding velocity.

The friction theory was first developed for metal rotating bands. Essentially the theory separates the heat, generated from fluid shear stresses, into the melting of one surface and into conduction for the non-melting surface. It was found that a negligible fraction of the heat went to melting (of the rotating band). Since conduction to the barrel predominates, it is the surface thermal properties of thermal conductivity and diffusivity that are important. The significant parameter for the melting band is the melting point temperature. During multiple firing conditions it is possible that hot propellant gases cause the barrel surface temperature to exceed the rotating band melting temperature. Then there would be conduction from the barrel to the melt which would add to the shear stress generating heat to melt the rotating band. The equations must be altered accordingly.

The metal melt was assumed to be Newtonian in behavior. Tentative agreement with the data of Montgomery for copper rotating bands in gun tests support this assumption. To further justify the overall approach, the theory was extended to pin-on-disk devices. A comparison was made between the theory and the Franklin Institute data for high speed sliding between several pairs at various loads and speeds. Good

agreement was achieved in this more strenuous test of the theory. At lighter loads and slower sliding speeds the pin coefficient of friction changed considerably. It was found that under these conditions the melt thickness was on the same order as the surface root-mean-square roughness and full film lubrication was not achieved. Typical melt thicknesses are approximately 10^{-5} inches. Although this was not a problem for the very smooth, engraved rotating bands, future work on melt lubrication should address the melt of microcontacts.

Non-Newtonian melt rheology substantially altered the theory when applied to plastic rotating bands. Generally, film thicknesses did not differ much from the metal melts, but this was caused by the limiting shear stress condition of the high loads and speeds; Newtonian theory with the high viscosity polymer melts produced unreasonable film thicknesses. Again, most shear generated heat goes to conduction. The most important parameter is the limiting shear stress of the melt which directly determines the coefficient of friction. Viscosity and shear modulus enter into film thickness calculations. These three parameters depend on the pressure and temperature of the melt. Unfortunately, this data for limiting shear stress and modulus is practically non-existent for polymer melts.

REFERENCES

1. Krier, H., and Adams, M. J., "An Introduction to Gun Interior Ballistics and a Simplified Ballistics Code," Interior Ballistics of Guns, Progress in Astronautics and Aeronautics, Vol. 66, (1979).
2. Fisher, E. B., Ibid.
3. Perrin, D., and Duke, S. "Barrel Life in High Rate of Fire Gatling Guns," Proceedings of the Tri-Service Gun Tube Wear and Erosion Symposium, U. S. Army Armament Research and Development Command, Dover, NJ, March, 1977.
4. Davis, D. M., "Review of the Air Force Program in Gun Barrel Life," Ibid.
5. Heiney, O. K., "Ballistics Applied to Rapid-Fire Guns," Interior Ballistics of Guns, Progress in Astronautics and Aeronautics, Vol. 66, (1979).
6. Baer, P. G., "Practical Interior Ballistic Analysis of Guns,", Ibid.
7. Fisher, E. B., and Trippe, A. P., "Mathematical Model of Center Core Ignition in the 175 mm Gun," Calspan Rept. VQ-5163-D-2, March, 1974.
8. Stiffler, A. K., "Rotating Band Loads and Friction Forces in Interior Ballistics," Int. J. Mech. Sci., 25, (1983), pp. 105-119.
9. Montgomery, R. S., "Friction and Wear at High Sliding Speeds," Wear, 36, (1979), 275-298.
10. Montgomery, R. S., "Surface Melting of Rotating Bands," Wear, 38, (1976), pp. 235-243.
11. Montgomery, R. S. "Projectile Lubrication by Melting Rotating Bands," Wear, 39, (1976), pp. 181-183.
12. Stiffler, A. K., "Friction and Wear with a Fully Melting Surface," J. of Tribology, 3, (1984), pp. 416-419.
13. Stiffler, A. K., "Melt Friction and Pin-on-Disk Devices," submitted for review to the J. of Tribology.
14. Bowden, F. P., and Tabor, D., Friction and Lubrication of Solids, Clarendon Press, Oxford, (1964).
15. McFarlane, J. S., and Tabor, D., "Relation Between Friction and Adhesion," Proc. Roy. Soc., A202, (1950), p. 224.

16. Shooter, K. V., and Tabor, D. "The Frictional Properties of Plastics," Proc. Phys. Soc., (London), 65B, (1952), p. 661.
17. Howell, H. G., and Mazur, J., "Amontons' Law and Fiber Friction," J. Text. Inst., 44, (1953), T59.
18. Pascoe, M. W., and Tabor, D., "The Friction and Deformation of Polymers," Proc. Roy. Soc., (London), A235, (1956), p. 210.
19. Adams, N., "Friction and Deformation of Nylon I. Experimental," J. Appl. Poly. Sci., 7, (1963), p. 2075.
20. Adams, N., "Friction and Deformation of Nylon II. Theoretical," J. Appl. Poly. Sci., 7, (1963), p. 2105.
21. Lodge, A. S., and Howell, H. G., "Friction of an Elastic Solid," Proc. Phy. Soc., (London), B67, (1954), p. 89.
22. Archard, J. F., "Single Contacts and Multiple Encounters," J. Appl. Phys., 8. (1961), p. 1421.
23. Cohen, S. C., and Tabor, D., "The Friction and Lubrication of Polymers," Proc. Roy. Soc., (London), A291 (1966), p. 186.
24. Rabinowicz, S., et al., "The Effect of Hydrostatic Pressure on the Shear Yield Behavior of Polymers," J. Mat. Sci., 5, (1970), p. 29.
25. Mears, D. R., et al., "Effects of Hydrostatic Pressure on the Mechanical Behavior of Polyethylene and Polypropylene", J. Appl. Phys. 40. (1969), p. 4229.
26. Bowden, P. B., and Jukes, J. A., "the Plastic Flow of Isotropic Polymers," J. Mat. Sci., 77, (1972), p. 52.
27. Briscoe, B. J., and Tabor, D., "The Effect of Pressure on the Frictional Properties of Polymers," Wear, 34, (1975), p. 29.
28. Sauer, J., "Deformation, Yield and Fracture of Polymers at High Pressure," Poly. Eng. Sci., 17, (1977), p. 150.
29. Towle, L. C., "Shear Strength and Friction Measurements on Thin Layers Under High Pressure," J. Appl. Phys., 42, (1971), p. 2368.
30. Towle, L. C., "Friction and Shear Strength of a Chromium Tris (Phosphinate) Polymer Under High Pressure," ASLE Trans., 17, (1974), p. 224.
31. Peterson, M. B., and Ling, F. F., "Frictional Behavior in Metalworking Processes," J. Lub. Tech., 92, (1970), p. 535.

32. Ludema, K. C., and Tabor, D., "The Friction and Visco-elastic Properties of Polymeric Solids," Wear, 9, (1966), p. 329.

33. Jaeger, J. C., "Moving Sources of Heat and Temperature at Sliding Contacts," Proc. Roy. Soc., (N.S.W.), 76, (1942), p. 203.

34. Archard, J. F., "The Temperature of Rubbing Surfaces," Wear, 8, (1965), p. 79.

35. Venogradov, G. V., et al., "A Study of Heavy Metal-to-Plastic Friction Duties and of the Wear of Hardened Steel in the Presence of Polymers," Wear, 8, (1965), p. 358.

36. McLaren, K. G., and Tabor, D., "Frition of Polymers at Engineering Speeds: Influence of Speed, Temperature and Lubricants," Wear, 8, (1965), p. 79.

37. Clerico, M., "A Study of the Friction and Wear of Nylon Against Metal," Wear, 13, (1969), p. 183.

38. Clerico, M., Tribological Behavior of Polyacetals", Wear, 64, (1980), p. 259.

39. Tanaka, K., and Uchiyama, Y., "Friction, Wear and Surface Melting of Crystalline Polymers," Advances in Polymer Friction and Wear, (ed., L. H. Lee), Vol. 5B, Plenum, New York, (1974), p. 499.

40. Tanaka, K., "Friction and Wear of Glass and Carbon Fiber-Filled Thermoplastic Polymers," J. Lub. Tech., 99. (1977), p. 408.

41. Herzfeld, C. M., and Kosson, R. L., "A Theory of Bore Friction," Report No. 851, Ballistic Research Laboratories, Aberdeen Proving Grounds, Maryland, (1953).

42. Wilson, W. R. D., "Lubrication by a Melting Solid," J. Lub. Tech., 98, (1976), p. 22.

43. Bicego, V., et al., "Lubrication of a Melting Slider Under Nonisothermal Conditions," J. Lub. Tech., 108, (1981), p. 436.

44. Johnson, R. L., et al., "Friction at High Sliding Velocities," NACA TN 1442, (1947).

45. Sternlicht, B., and Apkarian, H., "Investigation of Melt Lubrication," ASLE Trans., 2, (1960), p. 248.

46. Pinkus, O., and Sternlicht, B., The Theory of Hydrodynamics Lubrication, McGraw-Hill, New York, (1961).

47. Bowden, F. P., and Freitag, E. H., "The Friction of Solids at Very High Speeds," Proc. Roy. Soc., (London), A248, (1958), p. 350.

48. Bowden, F. P., and Persson, P. A., "Deformation, Heating and Melting of Solids in High Speed Friction," Proc. Roy. Soc., (London), A260, (1961), 433.

49. Landau, H. G., "Heat Conduction in a Melting Solid," Quart. J. Appl. Math., 8, (1950), p. 81.

50. Miller, D. R., "Friction and Abrasion of Hard Solids at High Sliding Speeds," Proc. Roy. Soc., (London), A269, (1962) p. 368.

51. Carignan, F. J., and Rabinowicz, E., "Friction and Wear at High Sliding Speeds," ASLE Trans., 24, (1980), p. 451.

52. Bradbury, D., et al., "Viscosity and Density of Lubricating Oils from 0 to 150,000 psig and 32 to 425°F," Trans. ASME, 73, 1951, pp. 667-676.

53. Glasstone, S., et al., "The Theory of Rate Proesses," McGraw Hill, 1941.

54. ASME Pressure-Viscosity Report, Vol. I-II, 1953.

55. Cameron, A., and Gohar, R., "Theoretical and Experimental Studies of the Oil Film in Lubricated Point Contact," Proc. Roy. Soc., Ser. A., 291, (1966), pp. 520-536.

56. So, B. Y. C., and Klaus, E. E., "Viscosity-Pressure Correlation of Lquids," ASLE Trans., 23, (1979), pp. 409-421.

57. Johnson, W. G., "A Method to Calculate the Pressure-Viscosity Coefficient from Bulk Properties of Lubricants," ASLE Preprint No. 80-AM-2E-2, (1980).

58. Allen, C. W., et al., "Elastohydrodynamic Lubrication of a Spinning Ball in a Nonconforming Groove," ASME Trans., J. of Lub. Tech., (1970), pp. 89-96.

59. Cheng, H. S., "Isothermal Elastohydrodynamic Theory for the Full Range of Pressure-Viscosity Coefficient," ASME Trans., J. of Lub. Tech., (1972), pp. 35-43.

60. Johnson, K. L., discussion of reference [13].

61. Klaus, E. E., and Fenske, M. R., Lub. Eng., 11, (1955), p. 107.

62. West, J. P., and Selby, T. W., "Effect of Engine Operation in Viscometric Properties of Multigraded Engine Oils," Mid-Year Meeting, SAE, (1965).

63. Milne, A. A., "A Theory of Rheodynamic Lubrication," Kolloid Z., Band 139, Heft 1/2, (1954), p. 6.

64. Milne, A. A., "A Theory of Grease Lubrication of a Slider Bearing," Proc. Second Intern. Congr. of Rheology, (1958).

65. Pinkus, O., and Sternlicht, B., "Theory of Hydrodynamic Lubrication," McGraw Hil, (1961).

66. Milne, A. A., "A Theory of Rheodynamic Lubrication for a Maxwell Liquid," Conf. on Lubrication & Wear, Paper 41, London, (1957).

67. Smith, F. W., "The Effect of Temperature in Concentrated Contact Lubrication," Trans. ASLE, 5, (1962), p. 142.

68. Johnson, K. L., and Cameron, R., "Shear Behavior of EHD Oil Films at High Rolling Contact Pressures," Proc. Inst. Mech. Engrs., London, 182, (1968), p. 307.

69. Barlow, A. J., and Lamb, J., "The Viscoelastic Behavior of Lubricating Oils Under Cyclic Shearing Stress," Proc. Roy. Soc., A253, (1959), p. 52.

70. Dyson, A., "Flow Properties of Mineral Oils in EHD Lubrication," Phil. Trans., A258, (1965), p. 529.

71. Dyson, A., "Frictional Traction and Lubricant Rheology in EHD Lubrication," Phil. Trans., A266, (1970), pp. 1-33.

72. Johnson, K. L., "Introductory Review of Lubricant Rheology and Traction," Proc. of the 5th Leeds-Lyon Sym. on Tribology, (1978), p. 155.

73. Ku, P. M. (ed.), "Interdisciplinary Approach to Liquid Lubricant Technology," NASA SP-318, (1972), pp. 187-262.

74. Hirst, W., and Moore, A. J., "EHD at High Pressures, II, Non-Newtonian Behavior," Proc. Roy. Soc., A360, (1978), pp. 403-425.

75. Johnson, K. L., and Roberts, A. D., "Observations of Viscoelastic Behavior of an EHD Lubricant Film, Proc. Roy. Soc., A337, (1974), pp. 217-242.

76. Alsaad, M., et al., "Glass Transitions in Lubricants: Its Relation to EHD Lubrication," ASME Trans., J. Lub. Tech., (1978), pp. 404-417.

77. Johnson, K. L., and Cameron, R., Proc. Instn. Mech. Engrs., 182, (1967), p. 307.

78. Hirst, W., and Moore, A. J., "Non-Newtonian Behavior in EHD Lubrication," Proc. Roy. Soc., A337, (1974), pp. 101-121.

79. Johnson, K. L., and Tevaarwerk, J. L., "Shear Behavior of EHD Oil Films," Proc. Roy. Soc., A356, (1977), pp. 215-236.
80. Rabinowitz, S., et al., "The Effect of Hydrostatic Pressure on the Shear Yield Behavior of Polymers," J. Mat. Sci., (1970), p. 29.
81. Mears, D. R., et al., "Effects of Hydrostatic Pressure on the Mechanical Behavior of Polyethylene and Polypropylene," J. Appl. Phys., 40, (1969), p. 4229.
82. Sauer, J., "Deformation, Yield and Fracture of Polymers at High Pressure," Poly. Engng. Sci., 17, (1977), p. 150.
83. Towle, L. C., "Shear Strength and Friction Measurements on Thin Layers Under High Pressure," J. Appl. Phys., 42, (1971), p. 2368.
84. Towle, L. C., "Friction and Shear Strength of a Chromium Tris (Phosphinate) Polymer Under High Pressure," ASLE Trans., 17, (1974), p. 224.
85. Bair, S., and Winer, W. O., "A Rheological Model for EHD Contacts Based on Primary Laboratory Data," ASME Trans., J. Lub. Tech., 101, (1979), pp. 258-265.
86. Bair, S., and Winer, W. O., "Some Observations in High Pressure Rheology of Lubricants," ASME Trans., J. Lub. Tech., 104, (1982), pp. 357-363.
87. Houpert, L., et al., "Rheological and Thermal Effects in Lubricated EHD Contacts," ASME Trans., J. Lub. Tech., 103, (1981), pp. 526-532.
88. Eyring, H., J. Chem. Phys., 4, (1936).
89. Han, C. D., Trans. Soc. Rheol., 18, (1974).
90. Mendlesc., R. A., Trans. Soc. Rheol., 9, (1965).
91. Parrini, P., Romanini, D., and Righi, G., Polymer, 19, (1976).
92. Mount, E. M., and Chung, C. I., "Melting Behavior of Solid Polymers on a Metal Surface at Processing Conditions," Poly. Eng. and Sci., 18, (1978), p. 711-720.
93. Cross, M. M., J. Appl. Poly. Sci., 13, (1969).
94. Bueche, F., and Harding, S., J. Poly. Sci. 32, (1958).
95. Vinogradov, G. V., et al., Dokl. Akad. Nank. SSSR, 154, (1964).
96. Graessley, W. W., J. Chem. Phys., 47, (1967).
97. Cogswell, F. N., "Polymer Melt Rheology: A Guide for Industrial Practice," Halsted Press, (1981).

98. Gross, W. A., "Film Lubrication," Report RJ117-8, IBM Corp., San Jose, Calif., (1960).

99. Constantinescu, V. N., Gas Lubrication," ASME, New York, (1969).

100. Landau, H. G., "Heat Conduction in a Melting Solid," Quart. J. Appl. Math., 8, (1950), p. 81.

101. Shugarts, W. W. and Rippel, H. C., "Frictional Resistance, Heating, and Wear at High Sliding Speeds," Final Report No. F-2448, The Franklin Inst., (1956).

102. Happel, J. and Brenner, H., "Low Reynolds Number Hydrodynamics," Prentice-Hall, (1965).

103. Rohsenow, W. M., and Hartnett, J. P., (eds.), "Handbook of Heat Transfer," McGraw-Hill Book Co., (1973).

104. Gupta, P. K., and Cook, N. H., "Statistical Analysis of Mechanical Interaction of Rough Surfaces," J. Lub. Tech., 94, (1972), p. 19-26.

105. Handbook of Thermophysical Properties of Solid Materials, Vol. 3, The MacMillan Co., (1961).

106. Conry, T. F., "Thermal Effects on Traction in EHD Lubrication," J. Lub. Tech., 103, (1981), p. 533-538.

(The reverse of this page is blank.)

INITIAL DISTRIBUTION

DTIC-DDAC	2
AUL/LSE	1
ASD/ENSZ (MR W E HARTLEY)	1
AFATL/CC	1
HQ USAF/SAMI	1
OO-ALC/MHWRB	1
AFIS/INT	2
ASD/ENESS (S. JOHNS)	1
HQ TAC/DRA	1
HQ USAF/DOQ	1
HQ PACAF/DOQQ	2
HQ TAC/INAT	1
ASD/XRX	1
USA TRADOC-SYS ANAL ACT	1
COMIPAC/PT-2	1
HQ PACAF/OA	1
USA BALL RSCH LAB/ARRADCOM	1
AFATL/CCN	1
AFATL/DLODL	2
AFATL/DLODA	1
FTD/SDNF	1
HQ TAC/XPS (STINFO)	1
USA MIS COMD/REDSTONE SCI INFO CTR	2
NAV RSCH LAB (CODE 2627)	1
NAV SYS COMD (TECH LIBR/AIR-004D4)	1
NAV WPNS EVAL FAC (CODE 81)	1
NAV WPNS CTR (CODE 3243)	1
AFATL/DLJG	10
NAV ORD SYS (CODE PM3A)	1
HQ AMCCOM (DOCE DRSMC-IRD(R))	1
USA ARM R&D CTR (DRSMC-LCE-D)	1
NAV AIR SYS COMD (CODE AIR 54111A)	1
BALL RSCH LAB (AMXBR-XAS)	1
ARRADCOM (LC/DR PICARD)	1
NAV WPNS CTR (CODE 32652/3265)	1
NAV SEA SYS COMD (CODE SEA-64E)	1
NAV WPNS CTR (TECH LIBR)	1

(The reverse of this page is blank.)

END

FILMED

3-85

DTIC